R-00-48

Sensitivity analysis of a discrete fracture network model for performance assessment of Aberg

Nils Outters
Golder Grundteknik KB

Dawn Shuttle
Golder Associates, Inc

December 2000

Svensk Kärnbränslehantering AB
Swedish Nuclear Fuel
and Waste Management Co
Box 5864
SE-102 40 Stockholm Sweden
Tel 08-459 84 00
+46 8 459 84 00
Fax 08-661 57 19
+46 8 661 57 19

ISSN 1402-3091
SKB Rapport R-00-48

Sensitivity analysis of a discrete fracture network model for performance assessment of Aberg

Nils Outters
Golder Grundteknik KB

Dawn Shuttle
Golder Associates, Inc

December 2000

Abstract

This report presents a sensitivity analysis of pathway simulations in a DFN model. The DFN model consists of two sets of stochastic fractures at different scales and the canister locations of a hypothetical repository layout. The hydrogeological base case model is defined by constant head boundary conditions on the edges of a 2000 x 2000 x 1000 m^3 block.

The pathway analysis carried out by the program PAWorks provides pathway parameters (pathway length, pathway width, transport aperture, reactive surface area, pathway transmissivity), canister statistics (average number of pathways per canister, percentage of canister locations with pathways) and visualisation of pathways.

The project provided the following results from the alternative cases:

- **Case 1**: Model with a 100 m thick fracture network at the repository scale instead of 50 m in the base case. The model is little sensitive to the increase of the thickness of the local fracture network.

- **Case 2**: Model including fracture networks where the mean size and size standard deviation is twice the ones used in the base case. The travel times to the biosphere is slightly shortened by increasing the fracture diameter.

- **Case 3**: Two models with alternative hydraulic boundary conditions: two different flux boundary conditions are tested instead of head boundary conditions in the base case. The advective travel time is shortened by changing the boundary conditions in both alternative cases; in some cases it is reduced to less than a year.

- **Case 4**: Study of alternative pathway search algorithms: the pathway search is here based on minimum travel time. The pathway search algorithm of PAWorks based on minimum travel time gives much more optimistic results than the base case where the maximum flow rate was used. The mean travel time is about 5000 years.

Due to editorial reasons only a subset of all this information is treated in this report.

Sammanfattning

Rapporten presenterar en känslighetsanalys för flödesvägsmodellering med hjälp av en DFN-modell. DFN-modellen består av två stokastiska spricksystem av olika skalor samt av deponeringshål för en hypotetisk förvarsanläggning. Randvillkor för det hydrogeologiska basfallet är definierat med konstant tryckhöjd på sidorna av ett 2000 x 2000 x 1000 m^3 stort block.

Flödesvägssökningen är gjord med programmet PAWorks. Programmet ger flödesvägsparametrar (flödesvägslängd, flödesvägsbredd, flödesvägstjockleken, reaktiv sprickyta, flödesvägstransmissivitet), deponeringshålsstatistik (antal deponeringshål med flödesväg) och flödesvägsvisualisering.

Känslighetsanalysen är baserad på flera alternativa fall. Fallen ger följande resultat:

- **Fall 1**: Modell med 100 m tjockt spricknätverk på anläggningsskala i stället för 50 m i basfallet. Modellen är endast svagt känslig för den ökade tjockleken av det lokala spricksystemet.

- **Fall 2**: Modell med spricknätverk vars sprickstorlek och standardavvikelse är dubbelt de i basfallet. Transporttiden till biosfären blir lite kortare med ökad sprickdiameter.

- **Fall 3**: Två modeller med alternativa hydrauliska randvillkor: två olika flödesrandvillkor är testade istället för tryckhöjdsvillkoret i basfallet. Transporttiden till biosfären blir lite kortare i de två alternativa randvillkorsmodellerna; i vissa fall är tiden kortare än ett år.

- **Fall 4**: Studie av alternativa sökalgoritmer för flödesvägar: sökningen är här baserad på kortaste transporttid. Fallet ger mycket mer optimistiska resultat än basfallet för vilket det maximala flödet användes. Transporttidens medelvärde blir 5000 år.

På grund av redigeringsskäl är bara en begränsad del av informationen presenterad i rapporten.

Table of contents

1 Introduction

1.1 Background

The Swedish Nuclear Fuel and Waste Management Company (SKB) is responsible for the safe handling and disposal of nuclear wastes in Sweden. This responsibility includes conducting studies into the siting of a deep repository for high-level nuclear waste. One important task of SKB is the overall long-term safety of a deep repository. This will include hydrogeologic modelling to examine the possible transport of radionuclides from the emplaced waste packages through the host rock to the accessible environment.

A modelling approach of transport is the discrete fracture network (DFN) model. This approach can provide key information concerning the formation characteristics of transport pathways.

An application of the discrete fracture pathways approach to the Aberg site within the context of the SR 97 Alternative Models Project was presented in SR-97 Alternative Models Project /Dershowitz et al, 1999/. This study demonstrated the use of the PAWorks pathway analysis approach for DFN models of the Aberg site within the SKB SR-97 PA project. The sensitivity of the DFN Pathway Approach will be presented here to emphasise the capacity of the DFN approach to quantify the variability in transport parameters and pathway geometry.

1.2 Scope of work

This report presents an extension of the discrete fracture pathways approach to the Aberg site within the context of the SR 97 Alternative Models Project (AMP) /Dershowitz et al, 1999/. This work will address the sensitivity of DFN pathway analysis to different parameters.

The variability in transport parameters in a number of realizations will be studied as a base case to estimate the minimum computing work required for a good statistical analysis.

The variability in transport parameters between the base case model and a model with different fracture set sizes will be studied to emphasise the importance of the size of local fracture networks in transport pathway formation.

The variability in transport parameters between the base case model and a model with modified statistical parameters will emphasise the importance of the confidence level in fracture statistical distribution.

The variability in transport parameters between the base case model and models with modified flow boundary conditions assumptions will be studied to understand how the DFN modelling approach can be integrated into other modelling studies based on a different modelling approach.

The variability in transport parameters between the base case model for which the pathways are identified by highest flow rate analysis and models with shortest travel time pathway identification will be studied. This should emphasise the advantage of the DFN approach over continuum models for which equivalency between identifications of pathway with highest flow rate and shortest travel time does not reflect the reality.

The hydrogeological model is defined by a 2000 x 2000 x 1000 m^3 rock block. Hydraulic boundary conditions are applied on the edges of the model. The repository is defined by canister locations, without any consideration for emplacement or access drifts. This model is implemented using discrete fracture statistical descriptions based on previous SKB reports /Uchida et al, 1994; Follin and Hermanson, 1996; Dershowitz et al, 1999/. These discrete fracture networks are then converted to approximately equivalent pipe networks, where the pipe networks are defined to have equivalent connectivity, flow rate, and transport properties as the plate fractures which they are representing. Flow simulations are carried out in the pipe network to determine the head field within the model. Finally, down-gradient pathways are identified from a representative percentage of the repository canisters to discharge boundaries, and the properties of these pathways are calculated.

The project used the following software:

- **FracMan/FracWorks**: Discrete fracture generation for stochastic fractures.
- **FracMan/GenPipes**: Converts fracture (2-D) networks to pipe (1-D) networks.
- **FracMan/EdPipe**: Assigns boundary conditions to pipe network.
- **FracMan/MAFIC**: Solves head fields within pipe networks consistent with prescribed head boundary conditions.
- **FracMan/PAWorks**: Identifies and characterises pathways through pipe networks, using graph theory algorithms.

2 Modelling approach

2.1 Fracture hydrogeology

Discrete fracture hydrogeology modelling is based on two fundamental empirical observations that flow and transport in geological materials are controlled by structural features and that the hydraulic conductivity of geological materials tends to follow a log normal or similarly skewed distribution.

As a result of the first observation, it is desirable to have a hydrogeological model which can model structural features to as fine a level of detail as possible. As a consequence of the second, it is possible to consider only a small portion of geological features. It has to be assumed that the vast majority of the geological material will not contribute significantly to the effective hydraulic properties, and can therefore be ignored. This leads to the use of a discrete fracture network (DFN) approach which concentrates on an accurate representation of conductive structures and flow barriers, sacrificing accuracy in the representation of smaller scale or less transmissive features.

The conceptual model used in the DFN approach assumes that discrete fractures provide the primary hydraulic flow paths and connections, and that accurate representation of flow path geometry is a key to successful hydrogeologic analysis. Discrete fractures may be fractures, faults, karsts, or paleochannels, depending on the scale and geology. Discrete fractures may be one, two, or three-dimensional features, but are generally modelled as polygons. Discrete fractures are generated in realistic three-dimensional networks based on structural geology and statistical information, and can be conditioned to local measurements. Interaction between discrete fractures and the rock matrix is represented using 1-D approximate dual-porosity approaches, true dual-permeability approaches, or is ignored altogether.

2.1.1 Assumptions and limitations

The key assumption and limitations of the DFN approach as applied in this project may be summarised as follows:

Assumption 1: The rock matrix permeability can be represented by a proportional increase in the transmissivity for a subset of all discrete features, without a significant loss in effective permeability or connectivity. The flow occurs through fracture planes, not the matrix.

Assumption 2: A range of scales of discrete features can be used to represent flow and transport behaviour at any scale.

Assumption 3: Discrete feature geometric and hydraulic properties can be derived from structural information and hydraulic tests.

Assumption 4: Discrete features can be represented by a combination of simple one, two, and three-dimensional structures such as plates, pipes, and prisms.

Assumption 5: Flow and transport in discrete features can be described by the same laws as used for continuum approaches (i.e., the Navier-Stokes and Darcy equations for flow).

Assumption 6: Meaningful boundary conditions can be defined and assigned to discrete features at the edge of the model.

Assumption 7: Discrete features that have not been intersected or measured can be described statistically based on those features that have been intersected and characterised.

Assumption 8: Problems can be described by a limited number of stochastic realizations of the fracture pattern.

Limitation 1: The number of discrete features that can be modelled is limited by available computational power. The number of discrete features necessary for hydrogeological modelling at a given scale may be greater than that which can be modelled.

Limitation 2: Data may be insufficient to provide appropriate statistics for stochastically generated features.

Limitation 3: Hydraulically significant features may have different properties from the geologically identified features used to generate statistics.

Limitation 4: More complex geological structures may be difficult to represent by simple geometric features.

Limitation 5: Matrix permeability may play an important role in connectivity. This is not considered in the present study

2.1.2 Governing equations

The governing equations assumed for flow in fracture planes are described in detail in the MAFIC User's Manual /Miller et al, 1994/. PAWorks uses 1-D finite elements in order to describe the pipe network. The equations for 1-D pipe flow used in this project are provided in Appendix A.

2.2 Pathways analysis

Performance assessment transport codes such as FARF31 /Norman and Kjellbert, 1990/ and RIP /Miller et al, 1996/ assume that groundwater transport in sparsely fractured crystalline rock can be simplified to a series of simple pipe pathways between the repository and the environmental "compliance boundary". These boundaries, at which doses to humans are calculated, may be the ground surface, specific geological features, or arbitrary surfaces, depending on the specific application.

In general, these simple pipe transport pathways are derived from continuum streamlines. By definition, streamlines assume steady state and a single fluid of constant density. However, the continuum streamline is not appropriate for fractured hard rocks such as those that are expected at many repository sites because the matrix flow is very

small compared to the flow in fractures. Therefore, a more sophisticated method for deriving transport path geometries and properties is required.

In fractured rock, the geometry of transport pathways is controlled by the geometry of discrete fractures. FracMan/FracWorks generates realistic, three-dimensional fracture geometries, and is therefore an appropriate method for deriving the pathways to be used in performance assessment calculations.

The approach used for the derivation of performance assessment pathways with PAWorks is described in detail in Dershowitz et al, 1999. First, FracMan/FracWorks is used to generate stochastic fracture geometries based on the reference site data. The geometry of the pathways to be considered then need to be defined in terms of sources and sinks. The sources and sinks may be defined as boreholes, planar surfaces or fractures. Boundary conditions are then assigned and a finite element method is used to calculate heads within the fracture network. In the current study, the pathway source is defined by the canister emplacement holes, and the sink is defined by the top surface of the model. PAWorks then follows the gradient within the fracture network from the source locations to the sink locations. PAWorks uses a graph theory search to identify and characterise pathways between the sources and sinks. Note that the pathway algorithm is following the local gradients within the fracture network, which may be different in direction and magnitude from the applied regional gradient.

Flow and transport through fracture networks is constrained to occur through 3-D networks of interconnected 2-D fractures (planes). However, PAWorks use 1-D pipes (lines) to represent transport. Appendix B describes the simplifications of the topology of the fracture network as applied in this project.

2.3 Pathway search

The pathway search algorithm is designed to identify the preferential pathways between specified sources and sinks. Preferential pathways are identified based on a combination of the geometry of the pipe network and a user assigned criteria.

Pathways are identified using a weighted, directed “priority first” graph algorithm. This search algorithm is based on Segdewick /1988/. The priority first search uses the weights on each pipe to determine the pathway which optimises the pathway criteria, and then looks for the pipe which is the second closest to matching that criteria. The search algorithm identifies a set of non-reentrant tree-branching paths, including the “highest priority” path, based on the criteria established by the user. The algorithm does not identify all combinations of possible paths. The weighted, priority order search is summarised as follows:

1. All pipes directly connected to the source are identified, and the pipe with the highest value of the user specified “priority” ranking is selected and marked. In the current study, the source is defined by the canister hole fractures, and the priority ranking is based on flow rate.

2. All of the unmarked pipes directly connected to the marked pipe are identified.

3. The process is repeated until either a dead end or the sink is reached. When the sink is reached, all of the pipes which make up the pathway are marked "visited".

4. As the pathway is identified, the pathway properties are calculated using the equations below.

PAWorks also offers the option to search different branches. Each canister had only one discharge point. The same starting point is used but at the first possible location a different branch than that for the previous pathway is chosen. This branch is followed using the same approach until the sink is reached. Branches are selected in order of the strength of the branch as a percentage of the flow rate entering the intersection. The process is repeated until the specified maximum number of branches or maximum number of pathways is reached.

Only the main branch with the highest flow rate was analysed. The current analysis defines path priority by flow rate, which provides results similar to those obtained by particle tracking. Alternatively, the path priority could be based on transmissivity, resistance, or travel time. The alternative of a pathway search based on travel time is presented in section 4.5.

2.4 Effective pathways

The pathway search algorithm identifies the individual pathways from sources to sinks. These pathways consist of multiple serial pipe elements. In the current study, an effective pathway is defined as a single homogeneous set of pipes connecting source to sink. Because different branches for the same starting pipe were not computed there is no need to average properties over different branches of a pathway. Hence, the effective properties of a pathway are only calculated from the series of pipes making up that pathway. Each pipe element represent the active flow part of a fracture.

One goal of PAWorks is to estimate the conductance, transmissivity, conductivity, and geometric properties of a representative pipe connecting source to sink. In the present study, PAWorks calculates these properties using individual and representative pathways as rectangular pipe channels (idealised to be between two parallel surfaces) of specific length, width, and aperture. The calculation details are shown in Appendix C.

2.5 Performance measures

The FracMan/PAWorks approach provides information about the pathways from the canister hole to the accessible environment, including the geometry of the pathway, the variation in velocity and geochemistry, and the location of discharge. However, for the purposes of the present project, only a few parameters directly related to the code **FARF31** and **COMP23** need be calculated.

They are namely:

- **F-factor**

  The normalised area along the pathway that is available for diffusion and sorption processes [TL^{-i}].

  The F-Factor F_{pipe} is calculated for each pipe as:

$$F_{pipe} = 2\, W_{pipe}\, L_{pipe}/Q_{pipe} \tag{2-1}$$

  where W_{pipe} is the pipe width [L], L_{pipe} is the pipe length [L], and Q_{pipe} is the pipe flow rate [L^3T^{-1}]. (See Appendix C).

  The effective F-Factor F_{path} for the pathway is calculated as the sum of the F-Factors F_{pipe} for all of the pipes that make up the pathway:

$$F_{path} = \sum F_{pipe} \tag{2-2}$$

- **Travel time**

  The advective residence time from a canister location to the environmental discharge [T].

  The travel time t_{pipe} for each pipe in each pathway is calculated as:

$$t_{pipe} = L_{pipe}\, a_{pipe}\, W_{pipe}\, /Q_{pipe} \tag{2-3}$$

  where L_{pipe} is the pipe length [L], a_{pipe} is the pipe aperture [L], W_{pipe} is the pipe width [L], and Q_{pipe} is the pipe flow rate [L^3T^{-1}].

  The travel time t_{path} for a pathway is calculated as the sum of the travel times for the pipes that make up the pathway:

$$t_{path} = \sum t_{pipe} \tag{2-4}$$

- **Darcy velocity**

  The velocity of the total flux from a canister location [LT^{-1}].

  The Darcy velocity q for each canister is calculated as:

$$q = Q_{pipe}/A \tag{2-5}$$

  where A is the area of the canister [L^2] and Q_{pipe} is the pipe flow rate [L^3T^{-1}].

2.5.1 Other parameters

It should be noted that the discrete fracture pathway approach could provide a variety of useful information in addition to the parameters above. For instance, for each pathway PAWorks can report pathway length, pathway width, pathway aperture, reactive surface area and transmissivity (see Appendix C).

3 DFN site model

This section describes the reference FracMan model used in the base case for the sensitivity analysis. It was originally developed for the AMP of SR 97. At the time of the AMP project, model simulations of the hydrogeology at Aberg have been performed on a regional scale by Svensson /1997/. Figure 3-1 shows the extent of the regional study as well as the location of the simulation domain for the AMP. The Äspö coordinates of the simulation domain are shown in Table 3-1. The size and location of the domain is chosen so that the discharge areas for the optimised layout will be in the centre /see Munier et al, 1997/.

Table 3-1. Äspö coordinates of the simulation domain to be used in the AMP /Ström and Selroos, 1997/.

Coordinate	Positive direction	Minimum	Maximum
x	East	+1000	+3000
y	North	+6000	+8000
z	Up	–1000	0

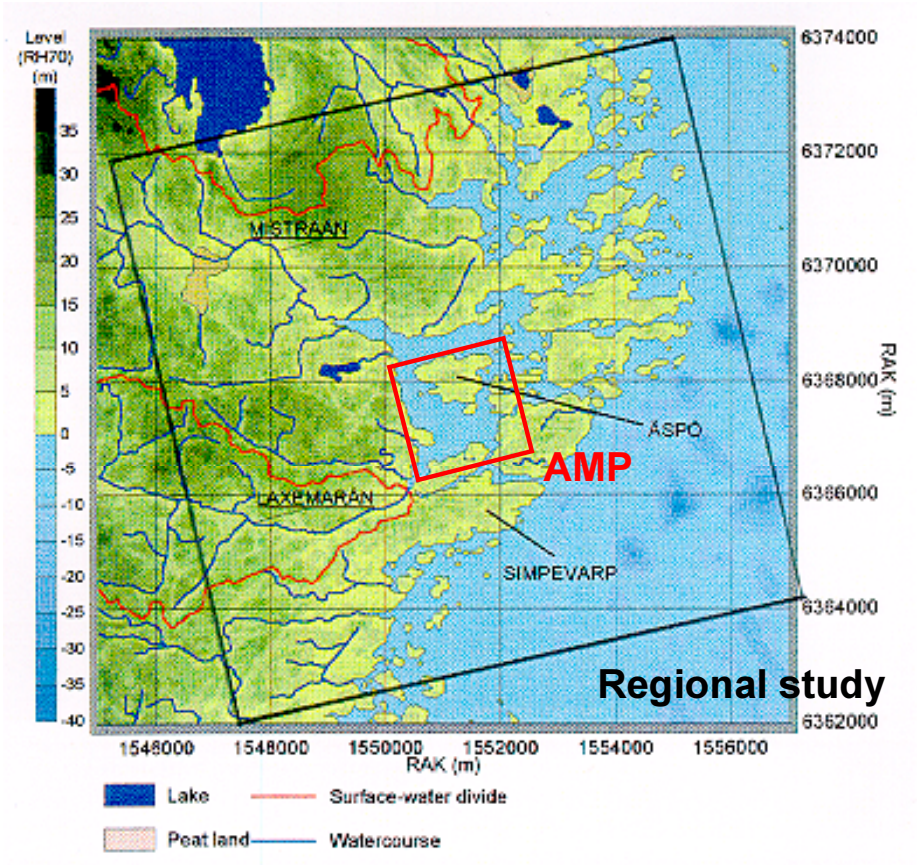

Figure 3-1. *Areal extent of the regional study by Svensson /1997/ as well as the location of the simulation domain for the AMP.*

To facilitate FracMan/PAWorks modelling, the model was divided into two fracture networks: one at the repository scale and one at the regional scale.

- **Regional scale**: The fracture generation region was established for the sake of the project as a 2000 m by 2000 m by 1000 m rock volume. Within this region, only fracture zones and the larger stochastic discrete fractures (model scale fractures) are simulated based on Rhén et al /1997/ and Uchida et al /1994/. Smaller stochastic fractures could not be modelled on a model scale due to computational constraints. Sensitivity studies carried out to determine the effect of this truncation is presented as case 1.

- **Repository scale**: The repository region was defined surrounding the repository sector. The detailed sector was defined to be large enough to provide a realistic representation of the connection from the canister emplacement boreholes to the surrounding fracture zones. This ensures both the correct hydraulic gradients through the repository area, and connectivity from the boreholes to the fracture zones for pathway formation. The repository region fracture statistics are based on Follin and Hermansson /1996/. Note that fractures from the larger stochastic fracture generation region also extend through the detailed model region.

The models regions are summarised in Table 3-2 below.

Table 3-2. Model regions simulated.

Geometric Feature	Regional scale	Repository scale
Region size	2000 m x 2000 m x 1000 m	800 x 700 x 50 m
Orientation of major axis (Äspö Coordinate System)	Trend θ= 0° Plunge ϕ = 0°	Trend θ= 0° Plunge ϕ = 0°
Orientation of minor axis (Äspö Coordinate System)	Trend θ= 90° Plunge ϕ = 0°	Trend θ= 0° Plunge ϕ = 0°
Centre of region (Äspö Coordinate System)	X_c = 2000E Y_c = 7000N Z_c = -500Z	X_c = 1850E Y_c = 7150N Z_c = -500Z
Features modelled	Fracture zones Stochastic fracture population with radius greater than 20 m	Emplacement canisters Stochastic fracture population with radius $0.2 \leq R \leq 20$ m

3.1 Rock mass parameters

The deterministic fracture zone geometry and transmissivity for this study was based solely on Rhén et al /1997/. The stochastic fracture geometry for this study was based primarily on TBM fracture statistics /Follin and Hermanson, 1996/, supplemented by larger scale outcrop fracture statistics /Uchida and Geier, 1992/. The rock mass parameters are presented in detail in Dershowitz et al, 1999.

Table 3-3 summarises the fracture model parameters considered in the DFN site model when modelling groundwater flow using FracMan. Appendix B describes the simplifications of the topology of the fracture network from 3-D networks of interconnected fractures to 1-D pipes (lines) as applied in this project.

Table 3-3. Rock mass parameters considered in the DFN model when modelling groundwater flow using FracMan.

DFN Parameter	Assumption	Basis
Regional scale	Box 2000 x 2000 x 1000 m^3	Ström and Selroos /1997/
Repository scale (around each sector)	Box 800 x 700 x 50 m	Aberg repository layout /Munier et al, 1997/
Conceptual model	BART (Enhanced Baecher)	TBM Trace maps Follin and Hermanson /1996/
Fracture orientation distribution	Bootstrap (κ=300) based on fractures mapped in the TBM tunnel	TBM Trace orientations (Terzaghi corrected) Follin and Hermanson /1996/
Fracture size distribution f(R) (Model region)	Lognormal Mean = 13.7 m Std.Dev = 12.7 m Truncated to 20 m ≤ R ≤ 1000 m	Uchida et al /1994/
Fracture size distribution f(R) (Repository region)	Lognormal Mean = 6 m Std.Dev = 3 m Truncated to 0.2 ≤ R ≤ 20 m	TBM Trace maps Follin and Hermanson /1996/
Termination probability	37%	TBM Trace maps Follin and Hermanson /1996/
Fracture transmissivity distribution f(T)	Truncated lognormal Mean = 9.0e-7 m^2/s Std.Dev. = 5.0e-6 m^2/s T_{min} = 1.0e-09 m^2/s	LPT-2 Data analysis /Uchida et al, 1994/
Conductive Intensity	P_{32} =0.2 m^{-1}	TBM Trace maps /Follin and Hermanson, 1996/
Conductive intensity (above T_{min} and R_{min})	P_{32} =0.038 m^{-1} (Model region) P_{32} =0.2 m^{-1}(Repository region)	Uchida et al /1995/
Transport aperture e_t	0.5 $T^{1/2}$	Doe /1993/

The derivation of fracture parameters is discussed in detail in Dershowitz et al /1999/.

3.2 Reference repository layout

The reference repository layout is the same as the layout of Sector 3 used in Dershowitz et al, 1999. The reference repository includes canister emplacement boreholes only, and does not consider drifts or shafts to have any hydrological significance. The canister dimensions are summarised in Table 3-4.

Table 3-4. Repository layout.

Parameter	Value
Canister locations	Sector 3, Dershowitz et al /1999/.
Number of canisters	500
Canister height	7.833 m
Canister diameter	1.75 m
Distance between canisters	6 m

The canisters representing the source locations for the pathway search, are modelled using a fracture group which consists of four fractures. The size of the four fractures was chosen so that the box formed by the fractures has the same volume as a canister. The centre of the box is identical to the centre of the canister.

Table 3-5 summarises the geometric characteristics of the implementation of the reference repository design in the current study.

Table 3-5. Repository model geometry.

"Canister" fractures	
Top	-500 m (Äspö coordinates)
No. of fractures per canister	4
Canister cross sectional area	2.4 m^2
Equivalent fracture box	1.55 x 1.55 m
Fracture length	7.833 m
Transmissivity	1.0 x 10^{-20} m^2/s

3.3 Boundary conditions

Svensson /1997/ carried out a regional, steady state variable-density flow simulation of the Äspö site using the PHOENICS continuum code. The results of Svensson's study are the basis for boundary conditions of the present study. For the purpose of this project, however, it was decided to use Svensson's fresh-water solution rather than the

variable-density solution. The results from this solution are fluxes to 100 m by 100 m panels, and as average fresh-water heads to 100 m by 100 m panels.

The discrete fracture network model uses the fresh-water head values (located in the centre of the panel) to define constant head boundaries. This is done by assigning fresh-water head to the boundary node using a parabolic distance weighted average of the 3 nearest head values.

4 Sensitivity of the DFN pathway approach

4.1 Introduction

An extensive series of DFN sensitivity studies is carried out. All sensitivity studies are based on a "base case model" for which different characteristics are changed one at a time. The geometry, material properties and boundary conditions of the base case model have been defined in Chapter 3. The sensitivity studies are namely:

- **Case 1**: Model with a 100 m thick fracture network at the repository scale instead of 50 m in the base case.
- **Case 2**: Model including fracture networks whose mean size and size standard deviation is twice the ones used in the base case.
- **Case 3**: Two models with alternative hydraulic boundary conditions: two different flux boundary conditions are tested instead of head boundary conditions in the base case.
- **Case 4**: Study of alternative pathway search algorithms: the pathway search is here based on minimum travel time.

Each alternative case is described in detailed in the sections below.

4.2 Case 1: Alternative local fracture set size

The DFN model of the repository is composed of two fracture networks: a regional fracture network and a local fracture network. The regional fracture network takes place within the whole modelled volume. The local fracture network is modelled as a slab located around the repository. The size of this slab is 800 x 700 x 50 m in the base case model. The alternative slab size is 800 x 700 x 100 m, which is twice as thick as in the base case model. This case is designed to control the sensitivity of the model to the size of the local fracture network. The modelling exercise should aim at handling as simple and small models as possible to reduce computing resources requirements and computing time.

4.3 Case 2: Alternative fracture mean size

A sensitivity analysis on the repository DFN model fracture size is carried out to study the variation in the network pathways. Fracture networks size is mainly defined by the fracture size distribution and the fracture density (expressed by P_{32}=Total fracture surface per unit volume). The fracture size distributions of the regional and local fracture networks have been described by Uchida et al /1994/ and Follin and Hermanson /1996/ respectively. Fracture size distributions have been interpreted as lognormal distribu-

tions. They are presented in the Table 4-1 below. Since the level of confidence in the P_{32} parameter is higher than the level of confidence in the log-normal distribution of fracture size, we assumed the P_{32} value constant and changed the mean and standard deviation of the regional and local fracture network distribution. The mean and standard deviation of the fracture radius is doubled. A decrease of the number of fractures over the whole model is observed.

Table 4-1. Parameters of the alternative fracture sets.

Fracture set	Original: truncated log-normal fracture distribution	Alternative: truncated log-normal fracture distribution
Regional scale set	Mean = 13.7 m Std.Dev = 12.7 m Truncation: 20 m≤R≤1000 m	Mean=**27.4 m** Std.Dev = **25.4 m** Truncation: 20 m≤R≤1000 m
Repository scale set	Mean = 6 m Std.Dev = 3 m Truncation: 0.2≤R≤20 m	Mean = **12 m** Std.Dev = **6 m** Truncation: 0.2≤R≤20 m

4.4 Case 3: Alternative flow boundary conditions

Ström and Selroos /1997/ specified that the model of the present study uses an explicit site-scale domain defined as a volume of 2000 m by 2000 m of areal extent, 1000 m in depth. The upper surface of the model is given at sea level (0 masl). The model is to rely on boundary conditions derived from the regional groundwater flow modelling study of Svensson /1997/.

The boundary conditions of the base case model integrates flow rates presented by Svensson, 1997. The values of the flow arrows indicate that recharge to the model domain occurs predominantly across the western boundary, whereas discharge from the model domain occurs predominantly across the top boundary. Hence, the overall flow pattern is that of recharge on the inland areas discharging to the coastal waters.

The sensitivity analysis consists in using simplified sets of boundary conditions. Two alternative sets of hydraulic boundary conditions are proposed.

- **Case 3a**: the first alternative consists in a recharge to the model across the western boundary (group flux: the sum of the flux of all nodes remains constant for the whole boundary) and a discharge across the top boundary /prescribed head, Svensson, 1997/. The remaining boundaries are assigned no flow conditions.

- **Case 3b**: the second alternative consists in a recharge to the model across the western boundary (group flux) and a discharge across the eastern boundary (group flux). The top boundary of the model is assigned to prescribed head /Svensson, 1997/ to set reference heads to the model. The remaining boundaries are assigned no flow conditions.

They two alternative boundary conditions are presented in Figure 4-1.

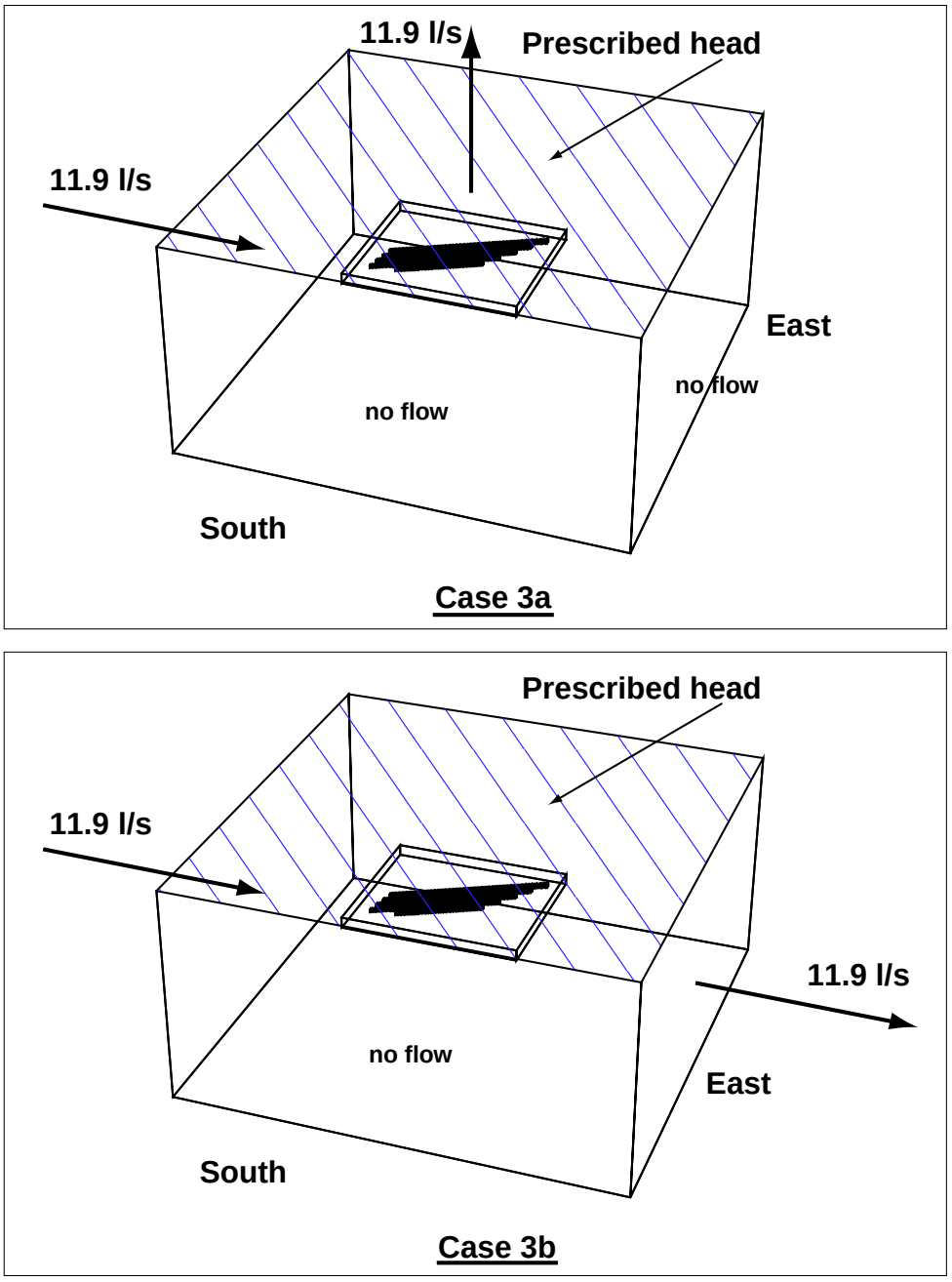

Figure 4-1. *Alternative flow boundary conditions.*

4.5 Case 4: Alternative search algorithms

For all realizations the pathway search was carried out on a canister-by-canister basis. The maximum number of pathways (per canister) was limited to one. Pathways were identified in the base case according to the maximum flow rate. It was alternatively identified using the “travel time weighted” pathway search in Case 4, and using the steady-state flow field derived by MAFIC 1D.

5 Results

5.1 Introduction

This section presents the results of the FracMan/PAWorks analysis carried out. A series of ten (10) stochastic realizations were carried out for the base case and each of the four alternative cases to identify and quantify transport properties of integrated scale pathways from canisters to the biosphere. This analysis integrates conventional near-field and far-field pathway approaches, since pathways are defined from canisters to the environmental release. These "performance measures" constitute statistics based on the base 10 logarithm of the F-factor (F_{path}), travel time (t_{path}) and Darcy velocity (q_c).

The hypothetical repository is composed of 500 canisters distributed in a horizontal plane. Since the pathway search is based on individual canisters, the 500 canisters were modelled in 5 different sets of 100 canisters each. They are namely Set 1, 2, 3, 4 and 5. They are presented in Figure 5-1 below.

Canister sets 1, 2 and 3 with 10 realizations each were modelled. An analysis of the results shows very little variation between the statistics of canister set 1 and the statistics of canister sets 1, 2 and 3. This analysis is presented in Appendix D. As a consequence, canister set 1 only was used in the different cases (Figure 5-2). For comparison purpose, the result tables of the cases are always presented together with the results of the base case. Results of the base case are based on the modelling of canister sets 1, 2 and 3.

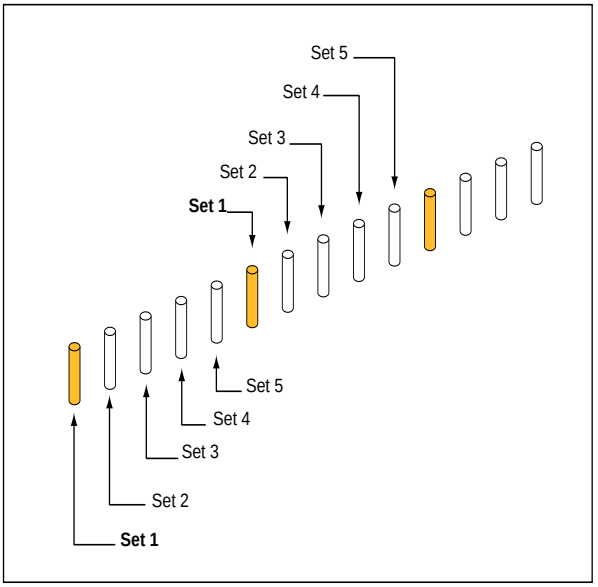

Figure 5-1. *Canister sets definition presented here for one row of canister.*

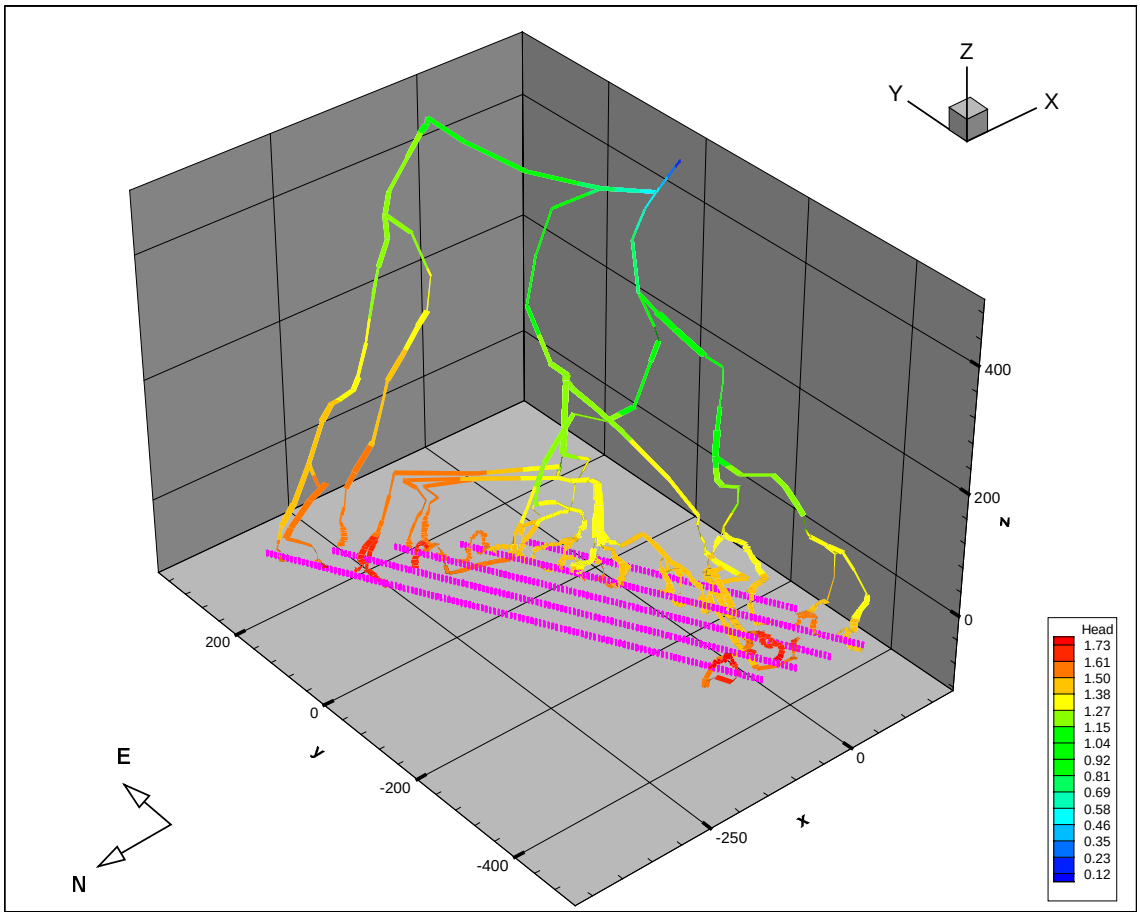

Figure 5-2. *Hypothetical repository with flow pathways from source to boundaries. Base case, realisation 00, fracture set 1.*

The following statistical entities are presented: mean, variance, median, standard deviation, range and percentage of canisters that are not connected with a boundary.

5.2 Comparison of the base case and AMP results

The rock mass parameters considered in the DFN model are the same as the parameters used in the SR97 Alternative Model Project except for the number of sectors considered. In the AMP, three canister sectors were considered at the repository level (sectors 3, 4 and 6). In the present project, only sector 3 is considered.

The pathway analyses are carried out in different ways in the two projects. In the AMP, the analysis allows several pathways to connect to a same canister. This is not the case in the present project where each canister may connect to a maximum of one flow pathway.

The comparison of the results between the two studies concerns the F-factor, the total travel time and the Darcy velocity.

Table 5-1. Comparison of pooled data between AMP and the results of the present study.

Stats	Log10 Travel time [yrs]	Log10 F-factor [yrs/m]	Log10 Darcy vel. [m/yrs]
Mean			
AMP	1.28	5.95	-2.46
Present study	1.50	5.20	-3.30
Standard deviation			
AMP	0.47	0.62	0.75
Present study	0.35	0.47	0.87
Median			
AMP	1.20	5.88	-2.43
Present study	1.48	5.18	-3.23

A first look at the Table 5-1 above indicate that the results of the AMP and the present study are relatively similar. This could be expected since there are only few constitutive differences between the two models.

However, a detailed comparison of the different entities of Table 5-1 above shows that the travel time is about 40% longer in the present study than in the AMP. This observation is consequent with the fact that the canister velocity (Darcy) is also slower in the present study. The calculated Darcy velocity is the sum of one or more pathway flux from a same canister, as required for a COMP31 analysis. The reason for differences in the results is that the number of pathways is limited to one in the present study and the mean of pathways per connected canister is about three in the AMP.

5.3 Case 1: Alternative size for the local fracture set

The complete set of results is presented in the tables in Appendix D.

The comparison of the mean of travel time shows that the connection to the boundaries of case 1 is slightly faster than for the base case. This was predictable, since the local fracture network around the canister location in case 1 is double as thick as in the base case. The probability of having high flow rate pipes in this region is higher.

The standard deviation of the travel time of case 1 is lower than in the base case. This is also due to a higher fracture density in the model that makes the travel time more uniform over the model.

The distribution of the F factor is very similar in both cases. This is illustrated by the histograms below.

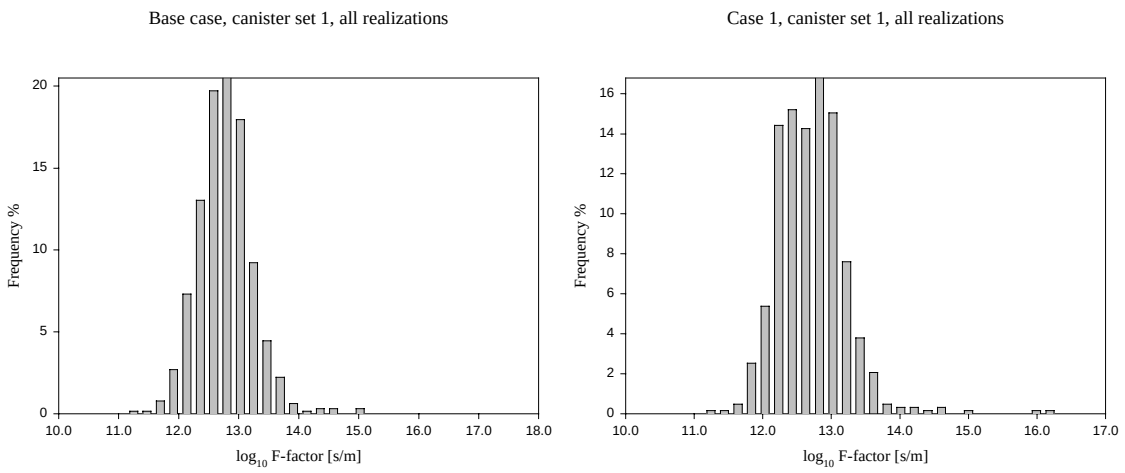

Figure 5-3. *Histograms of F-factor in base case and case 1.*

Scatter plots presented below and in Appendix D confirm that there is little variation between the base case and case 1. One should notice that F seems to be an exponential function of the travel time of the form $F=b.t^a$, where *a* and *b* are constant factors, as shown by Figure 5-4. In this case, a=1.75 and b=4.84. Parameters for linear and exponential fitting of F as function of time is presented in Appendix D.

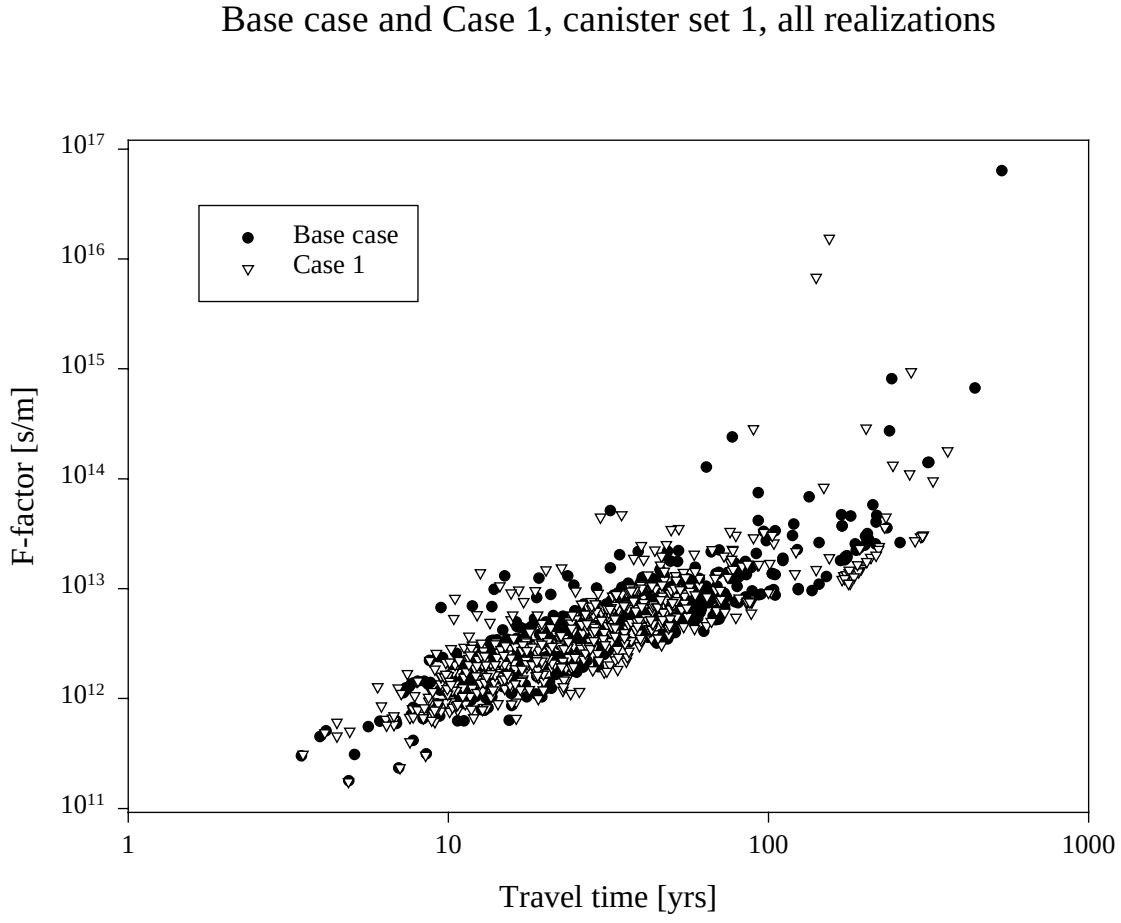

Figure 5-4. *F function of travel time in base case and case 1.*

The following conclusions can be drawn from case 1:

- Increasing the size of the local fracture network from 50 m thickness to 100 m does not influence the results a lot. Smaller models reduce computing time. For this reason, the size of the local fracture network will be kept at 50 m thickness for all the other cases.
- The travel time is shorter for case 1 than for the base case.
- The Darcy velocity is higher for case 1 than for the base case.
- The F factor is lower for case 1 than for the base case.
- The pathway lengths are longer in case 1 than in the base case.
- The connectivity of the fracture networks is unchanged.
- F can be assumed as an exponential function of the travel time.

5.4 Case 2: Alternative fracture size

The complete set of results is presented in the tables in Appendix D.

The comparison of travel times between the two cases shows that case 2 presents about 30% shorter travel times. This is illustrated by the histograms in Figure 5-5.

This observation is confirmed by the comparison of Darcy velocities that are slightly higher for case 2. Doubling the size of the fractures of the regional and the local networks slightly accelerates the migration of contaminant in the geosphere.

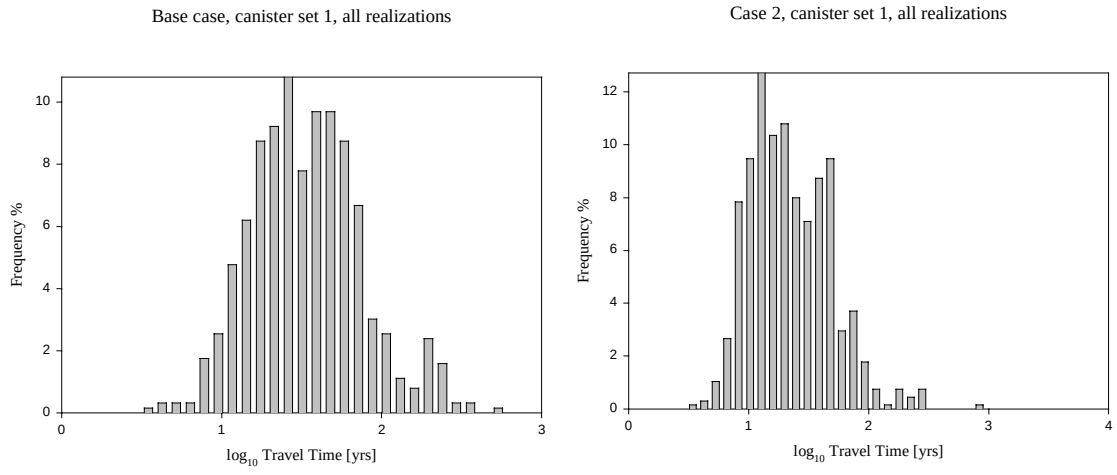

Figure 5-5. *Histograms of total travel time in base case and case 2.*

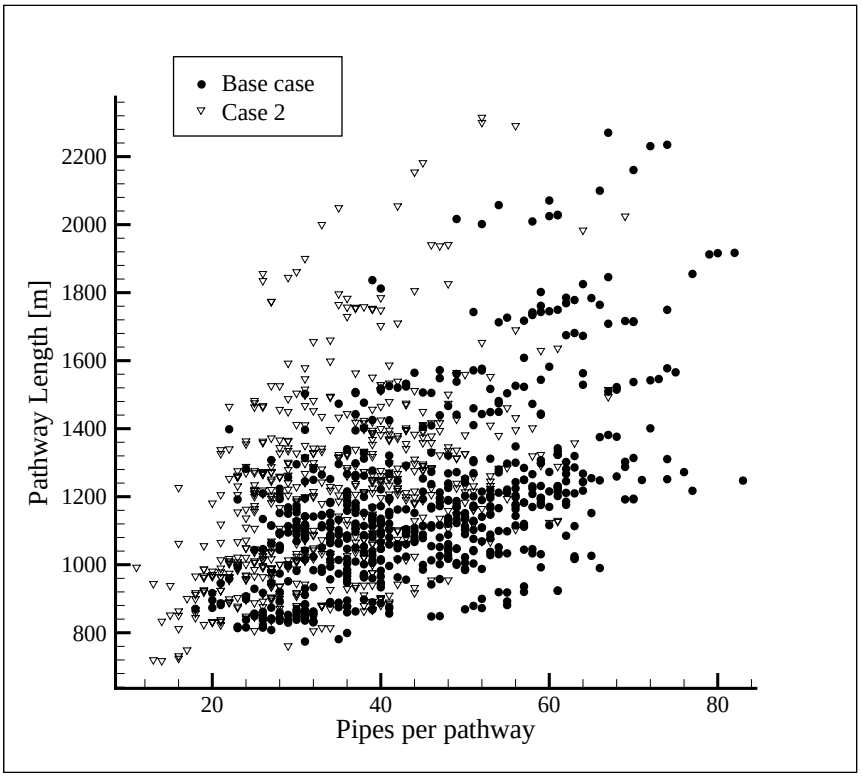

Figure 5-6. *Pathway length function of the number of pipes per pathways in base case and case 2, all realizations.*

It is observed that the F factor also shows lower values for case 2 than for the base case. F is a function of the pathway length and the flux. Figure 5-6 below shows that the pathway lengths are generally longer in case 2 than in the base case. However, this has no noticeable influence on F.

One can also notice that there are fewer pipes per pathway in case 2 than in the base case.

Scatter plots presented below and in Appendix D confirm that there is little variation between the base case and case 1. One should notice that F seems to be an exponential function of the travel time of the form $F=b.t^{a}$, as shown by Figure 5-7.

The following conclusions can be drawn from case 2:

- The travel time is shorter for case 2 than for the base case.
- The Darcy velocity is higher for case 2 than for the base case.
- The F factor is lower for case 2 than for the base case.
- The pathway lengths are larger in case 2 than in the base case.
- F can be assumed as an exponential function of the travel time.

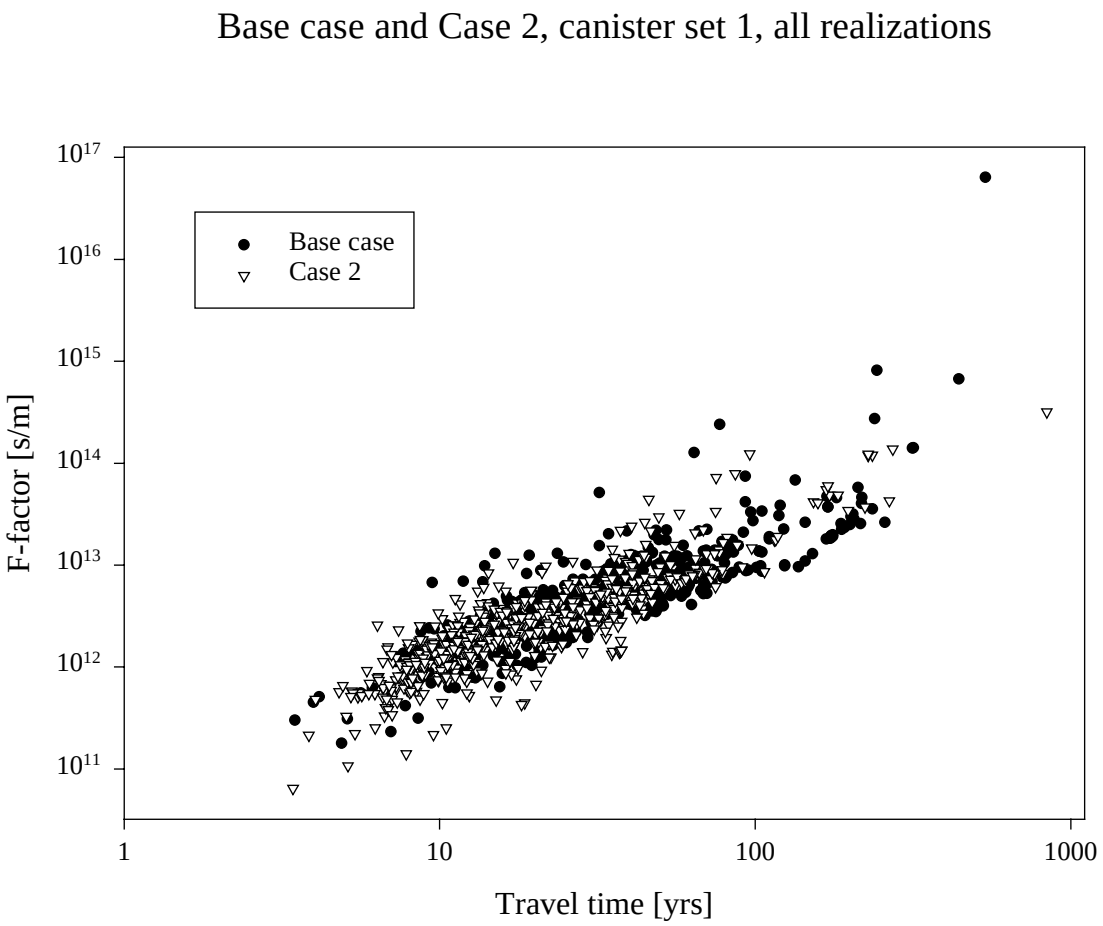

Figure 5-7. *F function of travel time in base case and case 2.*

5.5 Case 3: Alternative flow boundary conditions

The results of the comparison of the base case and case 3 are presented in the tables in Appendix D.

5.5.1 Case 3a: Inflow West, outflow Top

The comparison of travel times between the base case and case 3a shows that case 3a presents about 5 times faster travel times. This is illustrated by the histograms in Figure 5-8. This observation is confirmed by the fact that the Darcy velocity in case 3a is about 10 times higher than in the base case.

Comparison of the histograms of F factor for case 3a and base case shows a slightly lower F factor in the case 3a. However, the mean of the F factor is about 3 times lower than the mean of the base case. It can be explained by a higher standard deviation in the case 3a.

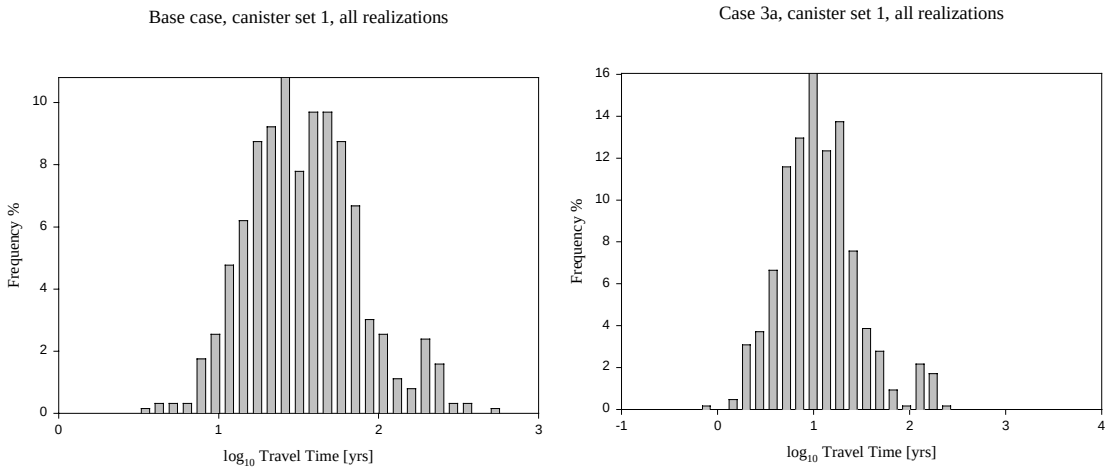

Figure 5-8. *Histograms of total travel time, base case and case 3a.*

The following conclusions can be drawn from case 3a:

- The travel time is 5 times shorter for case 3a than for the base case.
- The Darcy velocity is 10 times higher for case 3a than for the base case.
- The F factor is slightly lower for case 3a than for the base case with a higher standard deviation.

The hydraulic boundary conditions of case 3a are a simplification of the base case since flow takes place through two boundaries of the model only, and not six as in the base case. The direction of the flow is in case 3a imposed by the boundaries and it results in less dispersion in the flow paths. As a result, one can observe shorter travel time than in the base case. Even if the solution of case 3a is more conservative than the base case, the flow boundary conditions are less realistic than prescribed head boundary conditions.

5.5.2 Case 3b: Inflow West, outflow East

The comparison of travel times between the base case and case 3b shows that case 3b presents about 10 times faster travel times. The alternative case 3b also shows pathways with very short migration time of less than one year. This is illustrated by the histograms in Figure 5-9. This observation is confirmed by the fact that the Darcy velocity in case 3b is about 10 times higher than in the base case.

Comparison of the histograms of the F factor for case 3b and the base case shows a F factor reduced by almost a factor 10 in the case 3b. Moreover, the mean of the F factor is reduced by a factor 6 compared to the base case.

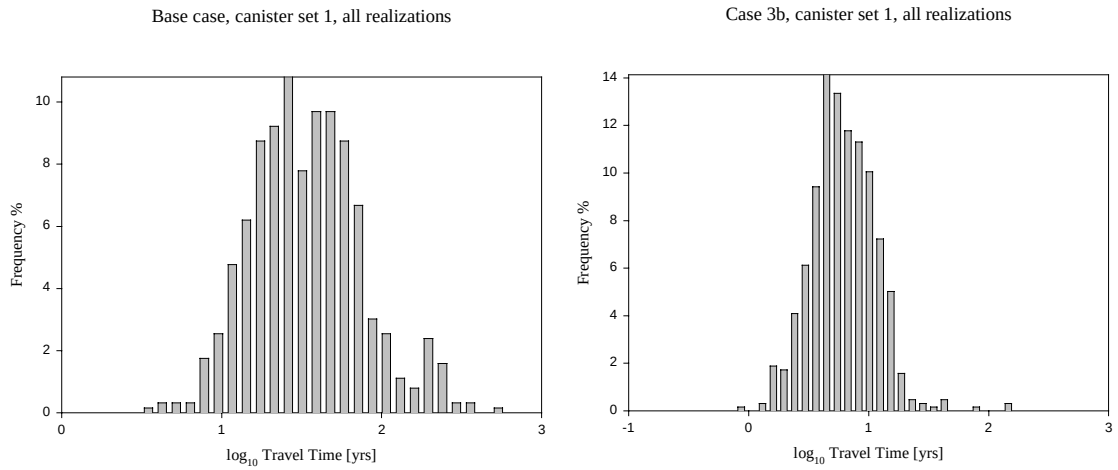

Figure 5-9. *Histograms of total travel time, base case and case 3b.*

The following conclusions can be drawn from case 3b:

- The travel time is 10 times shorter for case 3b than for the base case.
- Some pathways of case 3b have travel time less than one year.
- The Darcy velocity is 10 times higher for case 3b than for the base case.
- The F factor is lower for case 3b than the base case by a factor 6.

The boundary conditions of case 3b are also a simplification of the boundary conditions of the base case. Flow takes place between the western and eastern boundaries with prescribed flux. The direction of the flow is imposed by the boundaries and it results in less dispersion in the pathways. The pathway are therefore shorter than in the base case and case 3a since the distance between the eastern boundary and the canisters is shorter than between the canisters and the top of the model. This approach is conservative in the sense this is not an optimistic scenario. However, assigning no flow at all to the top of the model is not realistic.

5.6 Case 4: Travel time base pathway search

The models used in the base case and case 4 were identical in terms of geometry, fracture characteristics and boundary conditions. A pathway search algorithm based on minimum travel time was applied for case 4. Base case and case 4 show very different results. These differences concern all the performance measure parameters.

Case 4 presents two different types of pathways: one with low cumulative F factor and one with high cumulative F factor, see Figure 5-10 below.

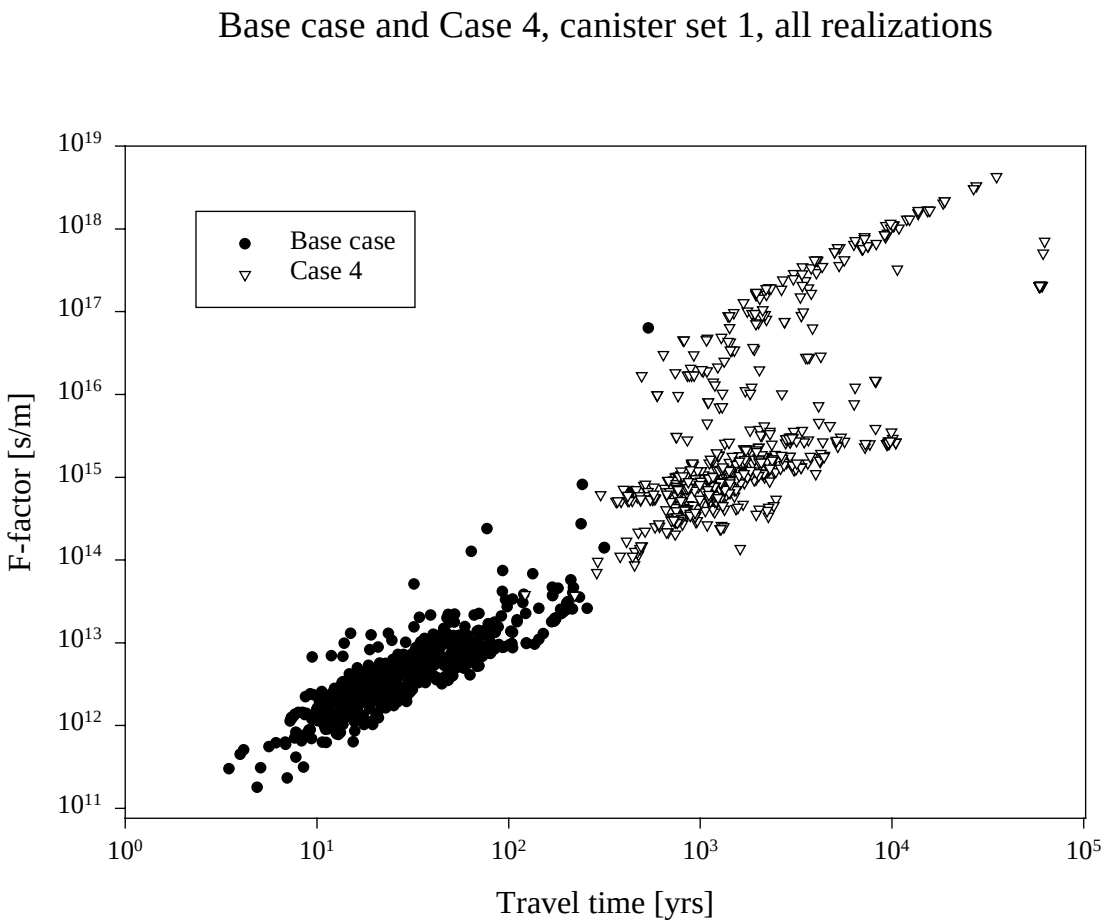

Figure 5-10. *Comparison of base case and case 4 F factor function of travel time.*

A detailed study of the pathways shows that there exists a few number of pipes in the model with much higher F factor than the rest of the pipes. This has been observed for all realizations. Since the performance measure chosen for this study is the cumulative F factor, all pipes downstream the pathway will have a cumulative F factor higher than any pipe upstream. This is illustrated by the plot of cumulative F-factor function of pathway length, Figure 5-11, where high F-factor values are reached at short distances of the canister locations.

The comparison between the base case and case 4 of the histograms of the F factor shows that the group of pathways with lowest F factor has an F factor 100 times the base case. Result tables give a mean F factor of about 10^{17} s/m for case 4 compared with 10^{14} s/m for the base case. The second group of pathways with high F factor has a large range of values, and its median is about 10^{17} s/m, see Figure 5-12.

The Darcy velocities at the canister are slightly lower for case 4 than base case. Small differences were expected since the geometry and the boundary conditions are the same in both models, only pathways from canisters are different.

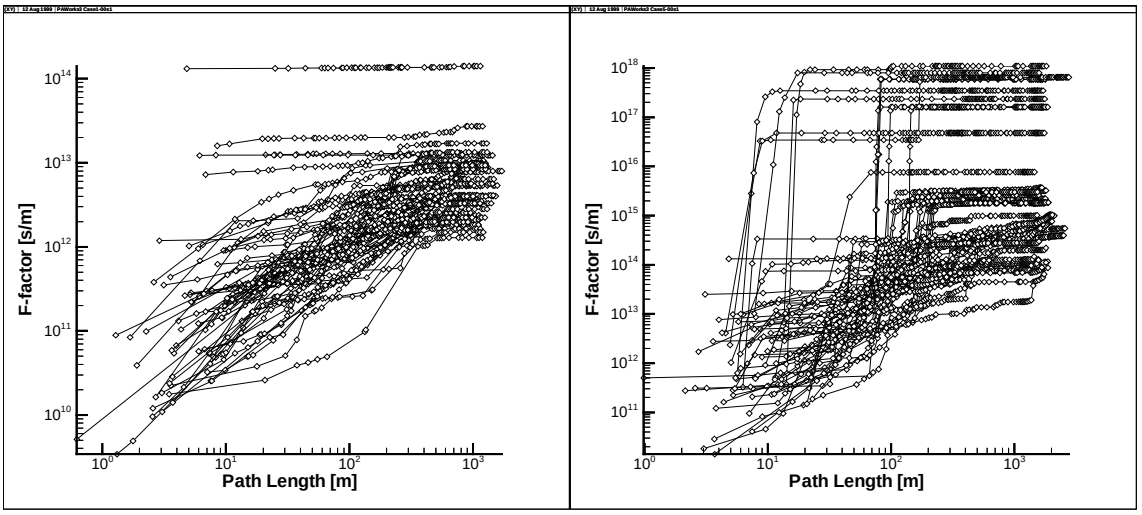

Figure 5-11. *F-factor and travel time, function of the distance from the canister sources. Base case (left) and Case 4 (right), fracture set 1.*

The comparison of the travel times between the two cases shows large differences. The mean travel time of case 4 is about 5000 years, compared to the base case mean travel time of 50 years. This can be explained by the fact that there are fewer pipes per pathway in the base case than in case 4. This is illustrated by Figure 5-13 below. The base case is characterised by pathways with few pipes with high flux. Case 4 is characterised by pathways with a large number of pipes selected for their low travel time. For one pathway, however, the sum of travel times of the pipes is larger than in the base case. This make the 'lowest travel time' search algorithm a non-conservative pathway search algorithm and thus should not be used for performance assessment.

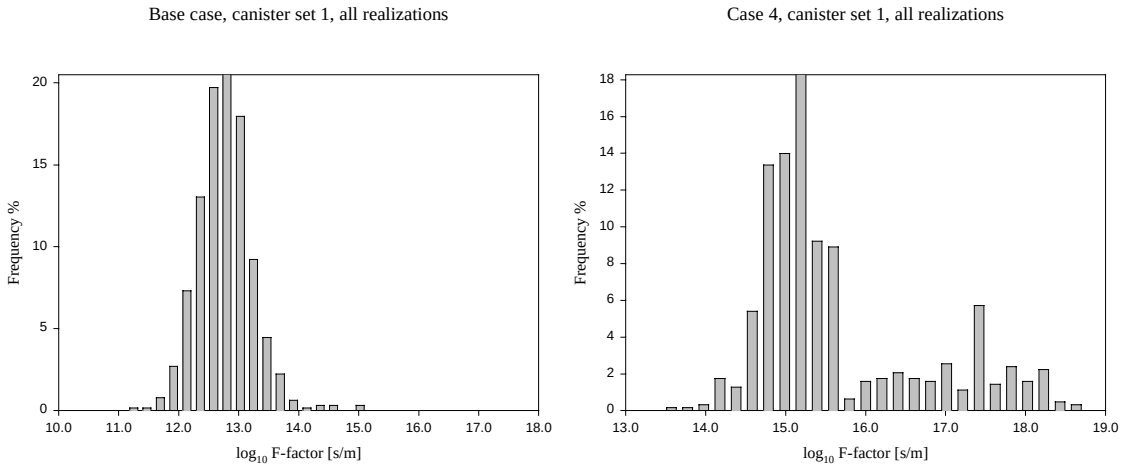

Figure 5-12. *Comparison of the F factor histograms, base case and case 4.*

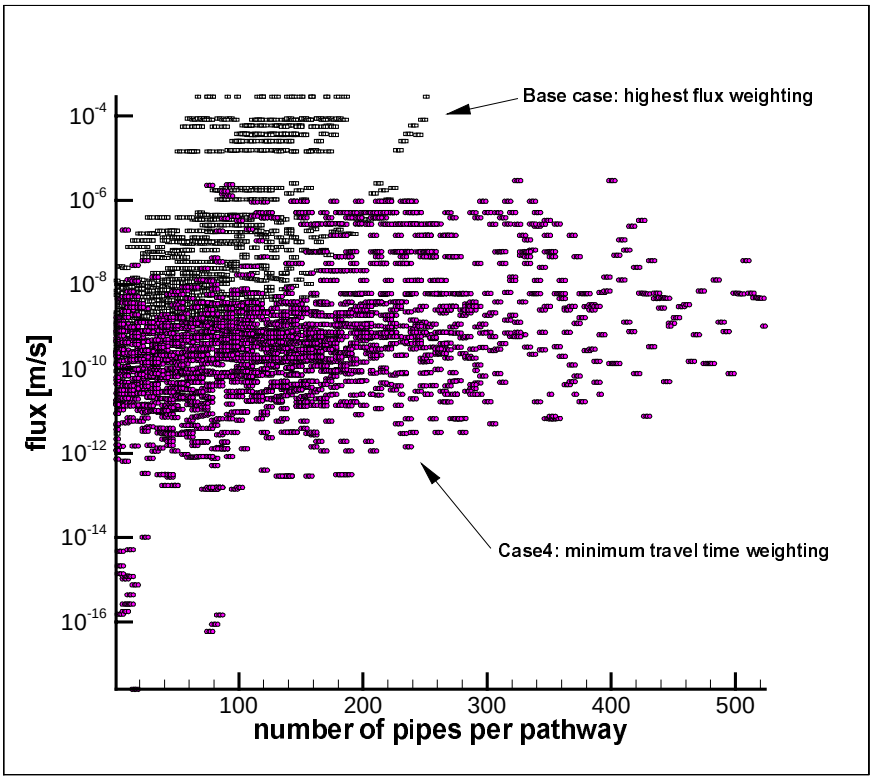

Figure 5-13. *Comparison of the number of pipes per pathway between base case and case 4.*

The following conclusions can be drawn from case 4:

- There exists a few pipes in the model with high F factor.
- Simulations based on travel time pathway search algorithm give more optimistic results than with highest flow search algorithm, with a mean travel time of about 5000 years.
- Simulations based on travel time pathway search algorithm generate solutions with a large number of pipes per pathways. The solution is less conservative than for the base case and thus should not be used for performance assessment.

6 Conclusions

This report presents a sensitivity analysis of pathway simulations in a DFN model. The DFN model consists of two sets of stochastic fractures at different scales and the canister locations of a hypothetical repository layout. The sensitivity analysis is based on several alternative cases. These cases consider changing of parameters in a base case. The pathway analysis carried out by the program PAWorks provides pathway parameters (pathway length, pathway width, transport aperture, reactive surface area, pathway transmissivity), canister statistics (average number of pathways per canister, percentage of canister locations with pathways) and visualisation of pathways.

The project provided the following results:

- **Case 1**: Model with a 100m thick fracture network at the repository scale instead of 50m in the base case. The model is little sensitive to the increase of the thickness of the local fracture network.

- **Case 2**: Model including fracture networks whose mean size and size standard deviation is twice the ones used in the base case. It is understood as a small perturbation of the initial model. The travel time the biosphere is slightly shortened by increasing the fracture diameter.

- **Case 3**: Two models with alternative hydraulic boundary conditions: two different flux boundary conditions are tested instead of head boundary conditions in the base case. The travel time of contaminants is shortened by changing the boundary conditions in both alternative cases; in some cases it is reduced to less than a year.

- **Case 4**: Study of alternative pathway search algorithms: the pathway search is here based on minimum travel time. The pathway search algorithm of PAWorks based on minimum travel time gives much more optimistic results than the base case. The travel time mean is 5000 years. This alternative should not be considered in safety assessment analysis.

Due to editorial reasons only a subset of all this information is treated in this report.

7 Acknowledgements

The author acknowledges the support of Power Reactor and Nuclear Fuel Development Corporation (PNC), and in particular Masahiro Uchida, for development of the initial PAWorks code. The author also acknowledges our colleagues Bill Dershowitz and Glori Lee for key technical contributions. Johan Andersson is acknowledged for the technical review of the report. Finally, the author acknowledges the Swedish Nuclear Fuel and Waste Management Co for ongoing support for application of discrete feature approaches within the Swedish radioactive waste management program.

G:\kt\rapp\R-2000\R-00-48\Manus\Wordtext\7.doc

References

Dershowitz W, Follin S, Andersson J, Eiben T, 1999. SR97 Alternative model project. Discrete fracture network modelling for performance assessment of Aberg. SKB International Cooperation. SKB R-99-43, Swedish Nuclear Fuel and Waste Management Co.

Doe T, 1993. Derivation of fracture transport aperture. Unpublished MS. Golder Associates Inc., Seattle.

Follin S, Hermanson J, 1996. A discrete fracture network model of the Äspö TBM tunnel rock mass. SKB AR D-97-001, Swedish Nuclear Fuel and Waste Management Co.

Miller I, Kossik R, Cunnane M, Hachey J, Keizur A, Shuttle D, 1996. RIP – Performance assessment and strategy evaluation model. Theory manual and user's guide. Golder Associates Inc, Seattle.

Miller I, Lee G, Dershowitz W, Sharp G, 1994. MAFIC – Matrix/ Fracture interaction code with solute transport. User documentation, version 1.5. Golder Associates Inc. report 923–1089. Golder Associates Inc., Seattle.

Munier R, Sandstedt H, Niland L, 1997. Förslag till principiella utformningar av förvar enligt KBS-3 för Aberg, Beberg och Ceberg. SKB R 97-09, Swedish Nuclear Fuel and Waste Management Co.

Norman S, Kjellbert N, 1990. FARF31 – A far-field radionuclide migration code for use with PROPERT. SKB TR-90-01, Swedish Nuclear Fuel and Waste Management Co.

Rhén I, Gustafson G, Stanfors R, Wikberg P, 1997. Äspö Hard Rock Laboratory – Geoscientific evaluation 1997/5. Models based on site characterization. SKB Technical Report TR 97-06, SKB, Stockholm.

Segdewick R, 1988. Algorithms, Second Edition, Addison-Wesley.

Ström A, Selroos J-O, 1997. SR 97 – Use of alternative models for describing flow and transport in the far field (CN, SC, and DFN), SKB PM 1997-04-25, Swedish Nuclear Fuel and Waste Management Co.

Svensson U, 1997. A regional groundwater model of the Äspö area. SKB TR 97-05, Swedish Nuclear Fuel and Waste Management Co.

Uchida M, Geier J, 1992. Fracture mapping on Äspö island. SKB SICADA Database, Swedish Nuclear Fuel and Waste Management Co.

Uchida M, Doe T, Dershowitz W, Thomas A, Wallmann P, Sawada A, 1994. Discrete-fracture modelling of the Äspö LPT-2, large-scale pumping and tracer test. SKB ICR 94-09, Swedish Nuclear Fuel and Waste Management Co.

Uchida M, Doe T, Sawada A, Dershowitz W, Wallmann P, 1995. FracMan discrete fracture modelling for the Äspö tunnel drawdown experiment. SKB ICR-96-22, Swedish Nuclear Fuel and Waste Management Co.

Appendix A: Governing flow equations

The governing equations assumed for flow in fracture planes are described in detail in the MAFIC User's Manual /Miller et al, 1994/. PAWorks uses 1-D finite elements in order to describe the pipe network.

A.1 Pipe element

The approximate head solution, $\hat{h}^e$, of a pipe element, e, can be expressed in a simple linear form:

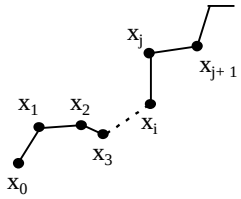

$$\hat{h}^e = a + bx \tag{A-1}$$

The coefficients a and b are determined from two nodal heads, h_i and h_j of the element, e, that has two ends at $x=x_i$ and $x=x_j$.

$$\begin{cases} h_i = a + bx_i \\ h_j = a + bx_j \end{cases} \tag{A-2}$$

$$\Rightarrow \begin{cases} a = \dfrac{x_j}{x_j - x_i} h_i - \dfrac{x_i}{x_j - x_i} h_j \\ b = \dfrac{-1}{x_j - x_i} h_i + \dfrac{1}{x_j - x_i} h_j \end{cases} \tag{A-3}$$

Equation A-1 can be rewritten as:

$$\hat{h}^e = \xi_i h_i + \xi_j h_j \tag{A-4}$$

$$\text{with} \quad \xi_i(x) = \frac{x_j - x}{x_j - x_i} \quad \text{and} \quad \xi_j(x) = \frac{-x_i + x}{x_j - x_i} \tag{A-5}$$

The function $\xi_i(x)$ is a linear basis function of the node i.

A quadratic basis function usually provides a better solution than a linear function. Starting from a quadratic polynomial of $\hat{h}^e$, the similar derivations from Equation A-1 to Equation A-4 will lead to the following solution:

$$\hat{h}^e = \xi_i h_i + \xi_m h_m + \xi_j h_j \tag{A-6}$$

$$\text{with} \quad \begin{aligned} \xi_i &= 2\frac{x - x_m}{x_j - x_i}\frac{x - x_j}{x_j - x_i} \\ \xi_m &= -4\frac{x - x_i}{x_j - x_i}\frac{x - x_j}{x_j - x_i} \\ \xi_j &= 2\frac{x - x_m}{x_j - x_i}\frac{x - x_j}{x_j - x_i} \end{aligned} \tag{A-7}$$

where:

x_m= the midpoint of the pipe = ½(x_i+x_j),

h_m= Nodal head at $x=x_{m,\ and}$

ξ_m= basis function at $x=x_m$

In general, we can express the approximate solution as:

$$\hat{h}^e = \sum_{k=0}^{M} \xi_k h_k \tag{A-8}$$

The summation index M represents the degree of polynomial used in the basis functions.

A.2 Derivation of equations using Galerkin method

Using the same notions as in MAFIC User's Manual /Miller et al, 1994/, Section 2.2, the approximate solution, Equation A-3, will be derived for 1-D pipe flow.

Starting from the governing equation for the transient pipe flow:

$$S\frac{\partial h}{\partial t} - T\frac{\partial^2 h}{\partial x^2} = q \tag{A-9}$$

Apply the Galerkin method to the governing equation (Equation A-9):

$$\int_L \left(S\frac{\partial \hat{h}}{\partial t} - T\frac{\partial^2 \hat{h}}{\partial x^2} - q \right) \xi_n dx = 0, n = 1,2,K\,N. \qquad \text{(A-10)}$$

where:

$\hat{h}$ = the approximate solution of head,

N= total number of nodes, and

L= length of the domain.

In the Galerkin method, the residues of the governing equation, i.e., the term $\left(S\frac{\partial \hat{h}}{\partial t} - T\frac{\partial^2 \hat{h}}{\partial x^2} - q \right)$ in Equation A-10, weighted by each basis function, ξ_n, n=1, 2,...N, must be zero when integrated over the entire domain, L.

The second derivative term in Equation A-10 can be reduced to a first derivative by applying integration by parts:

$$\int_L -T\frac{\partial^2 \hat{h}}{\partial x^2}\xi_n dx = \int_L T\frac{\partial \hat{h}}{\partial x}\frac{d\xi_n}{dx} dx - \int_\Gamma T\left(\frac{\partial \hat{h}}{\partial x} u_x \right) \xi_n d\sigma \qquad \text{(A-11)}$$

where:

Γ= the boundary of the problem domain,

u_x= the component of a unit vector normal to the boundary, and

σ= an integration variable representing distance along the boundary.

Insert Equation A-11 into Equation A-10, the equation becomes:

$$\int_L \left(S\frac{\partial \hat{h}}{\partial t}\xi_n + T\frac{\partial \hat{h}}{\partial x}\frac{d\xi_n}{dx} \right) dx = \int_L q\xi_n dx + \int_\Gamma T\left(\frac{\partial \hat{h}}{\partial x} u_x \right) \xi_n d\sigma = Q_n \text{ , n=1,2,...N} \qquad \text{(A-12)}$$

The terms on the right-hand side of Equation A-12 represent the flow source term, q, weighted by ξ_n over the domain and the normal flux term, $T\left(\frac{\partial \hat{h}}{\partial x}u_x\right)$, weighted by ξ_n over the boundary. The total flux weighted by ξ_n is denoted by Q_n on the right-hand side of Equation A-12.

The integration over the entire domain L can be done element by element, i.e., the summation of integrals over individual element in the domain:

$$\sum_e \left[\int \left(S_e \frac{\partial \hat{h}^e}{\partial t} \xi_n + T_e \frac{\partial \hat{h}^e}{\partial x} \frac{d\xi_n}{dx} \right) dx \right] = Q_n \quad n = 1,2,K\ N \tag{A-13}$$

where:

S_e= Storativity of the element e, and

T_e= Transmissivity of the element e.

Introduce the approximate solution $\hat{h}^e$, derived in Equation A-8 into Equation A-13, the equation becomes:

$$\sum_{e=1}^{E} \int_{\lambda^e} \left\{ S_e \left[\sum_{k=0}^{M} \xi_k \frac{dh_k}{dt} \right] \xi_n + T_e \left[\sum_{k=0}^{M} \frac{d\xi_k}{dx} h_k \right] \frac{d\xi_n}{dx} \right\} dx = Q_n \quad n = 1, 2, K\ N. \tag{A-14}$$

where:

λ^e= the subdomain of the element e, and

E= total number of pipe elements.

In terms of the matrix notation Equation A-14 can be transformed to:

$$\sum_{e=1}^{E} D_{k,n}^e \frac{dh_k}{dt} + A_{k,n}^e h_k = Q_n \tag{A-15}$$

where D^e is the element storage matrix and A^e the element conductance matrix:

$$D^e_{k,n} = \int_{\ell^e} S_e \xi_k \xi_n dx$$

$$A^e_{k,n} = \int_{\ell^e} T_e \frac{d\xi_k}{dx} \frac{d\xi_n}{dx} dx \qquad \text{(A-16)}$$

The individual terms of $D^e_{k,n}$ and $A^e_{k,n}$ are found by evaluating the integration over element e in Equation A-16. The global matrices D and A are simply assembled from the sum of each individual element matrix, D^e and A^e. Equation A-15 in terms of the global matrices is:

$$\sum_{m=1}^{N} \left[D_{nm} \frac{dh_m}{dt} + A_{nm} h_m \right] = Q_n \qquad n = 1,2,K\ N \qquad \text{(A-17)}$$

This is same as the Equation 2-3 in the MAFIC manual.

References

Miller I, Lee G, Dershowitz W, Sharp G, 1994. MAFIC – Matrix/ Fracture interaction code with solute transport. User documentation, version 1.5. Golder Associates Inc. report 923–1089. Golder Associates Inc., Seattle.

Appendix B: Pipe approximation for fracture network topology

Flow and transport through fracture networks is constrained to occur through 3-D networks of interconnected 2-D fractures (planes). However, PAWorks use 1-D pipes (lines) to represent transport, which requires a significant simplification of the topology of the fracture network. This appendix describes the simplifications of the topology of the fracture network as applied in this project.

The approximation made here assumes that fractures (2-D) can be represented topologically as a system of pipes (1-D) interconnecting the fracture intersections on that fracture (Figure B-1, Step 2). The errors which result from this approximation illustrated in Figure B-1 include:

- double counting of conductance of portions of the fracture network where pipes intersect,
- ignoring portions of the fracture surface area which are not directly between fracture intersections,
- double counting of flow area for overlapping pipes, and
- channeling and spreading in each pipe is controlled by trace sizes, not by pressure streamlines within the fracture planes.

These errors have been assessed through comparison of plate flow MAFIC simulations to the pipe flow approximations /Shuttle et al, 1997/ and the conclusions have been implemented in the algorithm for generating networks of pipes from the plate fracture network. The algorithm as used in this project is as follows (Figure B-1):

1. Calculate intersections (traces) between all fractures in the fracture network and develop a linked list of fracture connections.
2. Within each fracture, define pipes depending on chosen criteria a), b), c) or d) (Figure B-2).
    a) All pipes that can be formed from the midpoints of the traces. The only restriction is that a new pipe cannot cross an existing one. Note that this algorithm is somewhat dependent on the sequence in which pipes are formed.
    b) Pipe generation identical to (a) apart from the additional restriction that pipes are not allowed to cross traces, and that each node (located at the mid-point of each trace) has at least one pipe connected.
    c) Pipes from (b) plus additional pipes to ensure that all pipes on the same fracture are connected to each other.

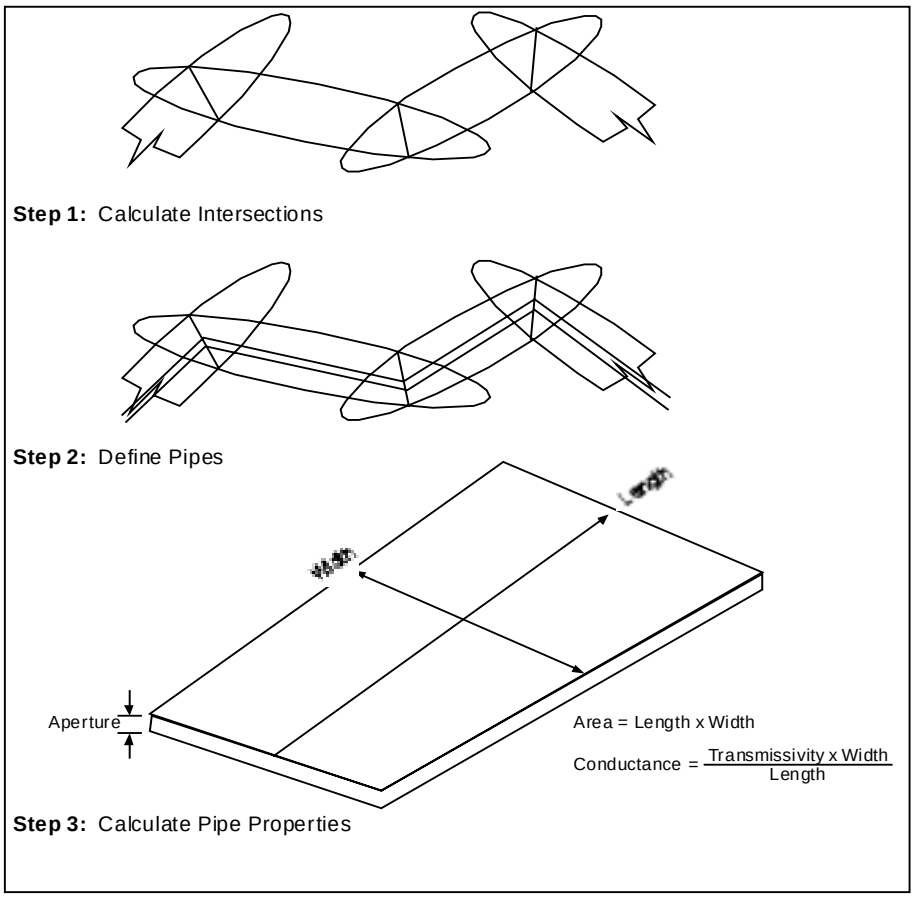

Figure B-1. *Pipe generation algorithm.*

d) Pipes from (c) plus effective pipes. An effective pipe will be formed when the pipe pathway distance between two nodes is greater than an effective pipe factor, N, times the cartesian distance between the nodes. The effective factor, N, is only used for Option d. The recommended range for N is between 1.2 to 3.0.

In the present study, option d) is used with an effective factor of 1.3.

3. For each resulting pipe the following properties are calculated:

a) Pipe length L: the distance between the trace centers.

b) Pipe width W: $W = X_{min} \cdot L_{min} + X_{max} \cdot L_{max}$
where:
L_{min} = length of the shorter trace
L_{max} = length of the longer trace
X_{min} = factor for the shorter trace (usually in the range 0-1)
X_{max} = factor for the longer trace (usually in the range 0-1)

For the present study, $X_{min} = X_{max} = 0.75$ is used based on the conclusions of Shuttle et al /1997/.

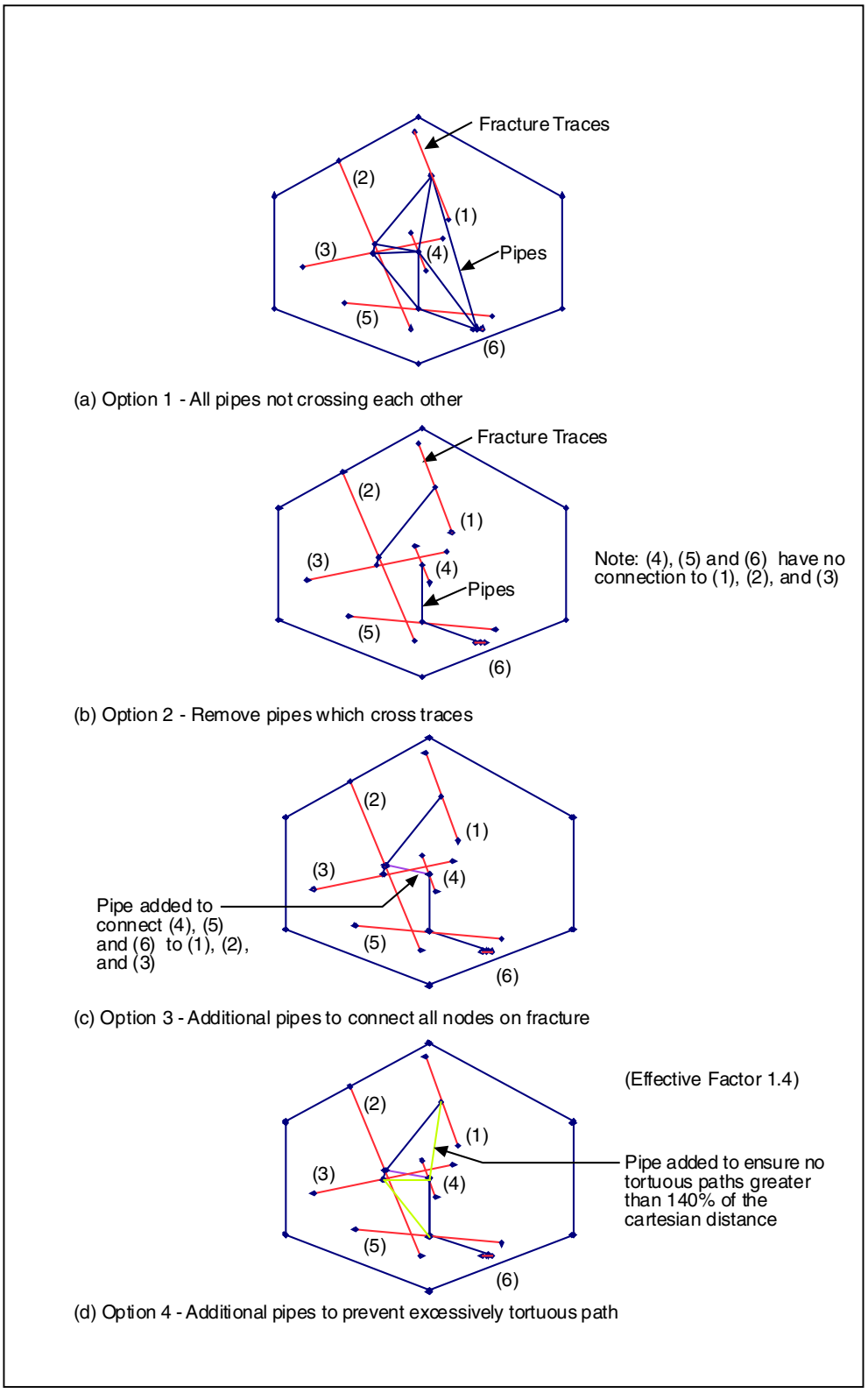

Figure B-2. *Pipe connectivity.*

c) Pipe transport aperture a: $a = a_1 \cdot (T)^{a_2}$
where:

T= Transmissivity of fracture

For the present study, $a_1 = 0.5$ and $a_2 = 0.5$ where used /Doe, 1993/.

d) Pipe surface area A: the surface area available for flow (W · L).

e) Pipe conductance C: the conductance for the pipe (W · T).

References

Shuttle D A, Dershowitz W, 1997. Analysis in Support of Performance Assessment. Technical Note, Golder Associates Inc., Seattle. Published as Appendix B of Dershowitz et al, 1998, Discrete Fracture Network Code Development, Heisei-8 Progress Report. Technical Report ZY 1597-97-001. Japan Nuclear Cycle Development Institute (JNC), Tokai, Japan.

Doe T, 1993. Derivation of fracture transport aperture. Unpublished MS. Golder Associates Inc., Seattle.

Appendix C: Effective pathway properties

One goal of PAWorks is to estimate the conductance, transmissivity, conductivity, and geometric properties of a representative pipe connecting source to sink. PAWorks can calculate these properties using two models:

1. The individual and representative pathways are fractures (idealized to be between two parallel surfaces) of specific length, width, and aperture (Figure C-1), or

2. The individual and representative pathways are cylindrical tubes of specific length and radius.

These models represent extremes of possible fracture flow behavior; it is likely that flow will neither be perfectly even as between two parallel plates nor completely channelized into a single cylindrical tube.

In this appendix effective pathway properties are calculated and reported based on the parallel plate model (Figure C-1).

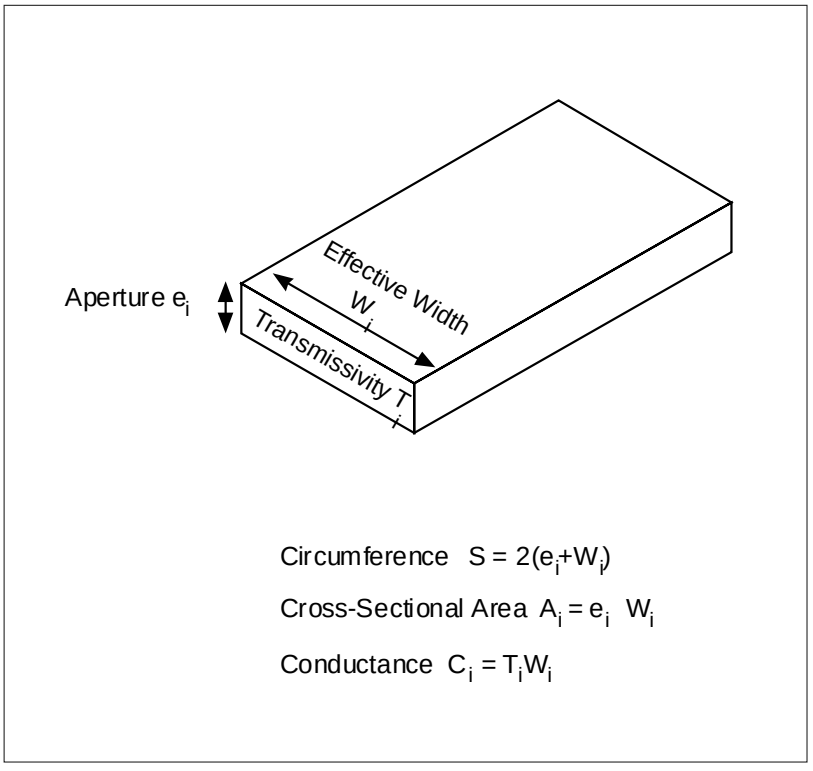

Figure C-1. *Parallel plate geometry schematic.*

Given Parameters

After the intersections and pipes are generated and the head values calculated, the following parameters are given for each pipe that is part of an identified pathway:

L_{pipe}	Length of each pipe, m
W_{pipe}	Width of each pipe, m
T_{pipe}	Transmissivity of each pipe, m^2/s
ΔH_{pipe}	Head drop over each pipe, m
ΔH_{path}	Head drop over entire pathway, m
t_{pipe}	Travel time of each pipe, s
Q_{pipe}	Flow rate in each pipe, m^3/s

Step #1: Calculate First Order Geometric Parameters

The effective path length is sum of the lengths of each component pipe:

$$L_{path} = \sum L_{pipe} \tag{C-1}$$

The effective path travel time is sum of the travel times of each component pipe:

$$t_{path} = \sum t_{pipe} \tag{C-2}$$

The effective pathway width, however, can obviously not simply be calculated as a sum of the pipe widths. Instead a weighted average is used:

$$W_{path} = \frac{\sum (W_{pipe} \cdot weighting\_property_{pipe})}{\sum weigthing\_property_{pipe}} \tag{C-3}$$

The weighting property used here depends on the user assigned pathway search criterium (e.g., flow rate).

Step #2: Calculate Pipe Hydraulic Gradients

The hydraulic gradient in each pipe as well as the entire pathway is the head drop per length:

$$i_{pipe} = \frac{\Delta H_{pipe}}{L_{pipe}} \tag{C-4}$$

$$i_{path} = \frac{\Delta H_{path}}{L_{path}} \tag{C-5}$$

Step #3: Calculate path conductivity

Knowing the pathway travel time, the pathway conductivity [m/s] is calculated as:

$$K_{path} = \frac{L_{path}}{t_{path} i_{path}} \quad \text{(C-6)}$$

Step #4: Calculate aperture, transmissivity and flow rate

This calculation is critical to the pathway property calculation. The three properties aperture, transmissivity and flow rate are interrelated, and which is computed first affects the overall pathway properties.

In the current study, the pathway aperture [m] is calculated first, as a flow rate weighted average:

$$a_{path} = \Sigma(a_{pipe} \cdot Q_{pipe})/\Sigma Q_{pipe} \quad \text{(C-7)}$$

Having computed the aperture, the transmissivity [m^2/s] and flow rate [m^3/s] are computed as follows:

$$T_{path} = K_{path} \cdot a_{path} \quad \text{(C-8)}$$

$$Q_{path} = K_{path} \cdot i_{path} \cdot W_{path} \cdot a_{path} \quad \text{(C-9)}$$

Alternative solutions are available in which transmissivity, pathway flow rate, or the flow rate at the exit element are calculated first:

The “transmissivity” option computes the pathway transmissivity first by weighting the transmissivity by the traversal property:

$$T_{path} = \frac{\sum (T_{pipe} \cdot weighting\_property_{pipe})}{\sum weigthing\_property_{pipe}} \quad \text{(C-10)}$$

Again, one of the triad of properties is defined the others follow from substitution:

$$a_{path} = T_{path} / K_{path} \quad \text{(C-11)}$$

$$Q_{path} = K_{path} \cdot i_{path} \cdot W_{path} \cdot a_{path} \quad \text{(C-12)}$$

The “flow rate” option computes the pathway flow first by weighting the flow by the traversal property:

$$Q_{path} = \frac{\sum (Q_{pipe} \cdot weighting\_property_{pipe})}{\sum weigthing\_property_{pipe}} \quad \text{(C-13)}$$

The apertures are then computed using the equation:

$$a_{path} = \frac{Q_{path}}{K_{path} \cdot i_{path} \cdot W_{path}} \quad \text{(C-14)}$$

where W_{path} is the pathway width, K_{path} is the hydraulic conductivity for the pathway, and i_{path} is the hydraulic gradient.

The "flow rate out" option computes the effective pathway aperture from the last value of flow rate on the pathway, using the equation:

$$a_{path} = \frac{Q_{out}}{K_{path} \cdot i_{path} \cdot W_{path}} \quad \text{(C-15)}$$

whith W_{path} as the pathway width, K_{path} as the hydraulic conductivity for the pathway, and i_{path} as the hydraulic gradient.

Step #5: Calculate reactive surface area

For calculation of the path surface area [m^2], three options are available (Figure C-2). The first is as the sum of all the individual fracture areas $A_{fracture}$ along the pathway:

$$RSA_{path} = \Sigma A_{fracture} \quad \text{(C-16)}$$

The second is as the sum of pipe areas A, i.e. the area calculated from the pipe width and length:

$$RSA_{path} = \Sigma (W_{pipe} \cdot L_{pipe}) \quad \text{(C-17)}$$

The third form of the fracture area is as:

$$RSA_{path} = \frac{\sum (W_{pipe} \cdot weighting\_property_{pipe})}{\sum (weigthing\_property_{pipe} \cdot L_{pipe})} \quad \text{(C-18)}$$

In the current study, the pipe area is calculated using the second option.

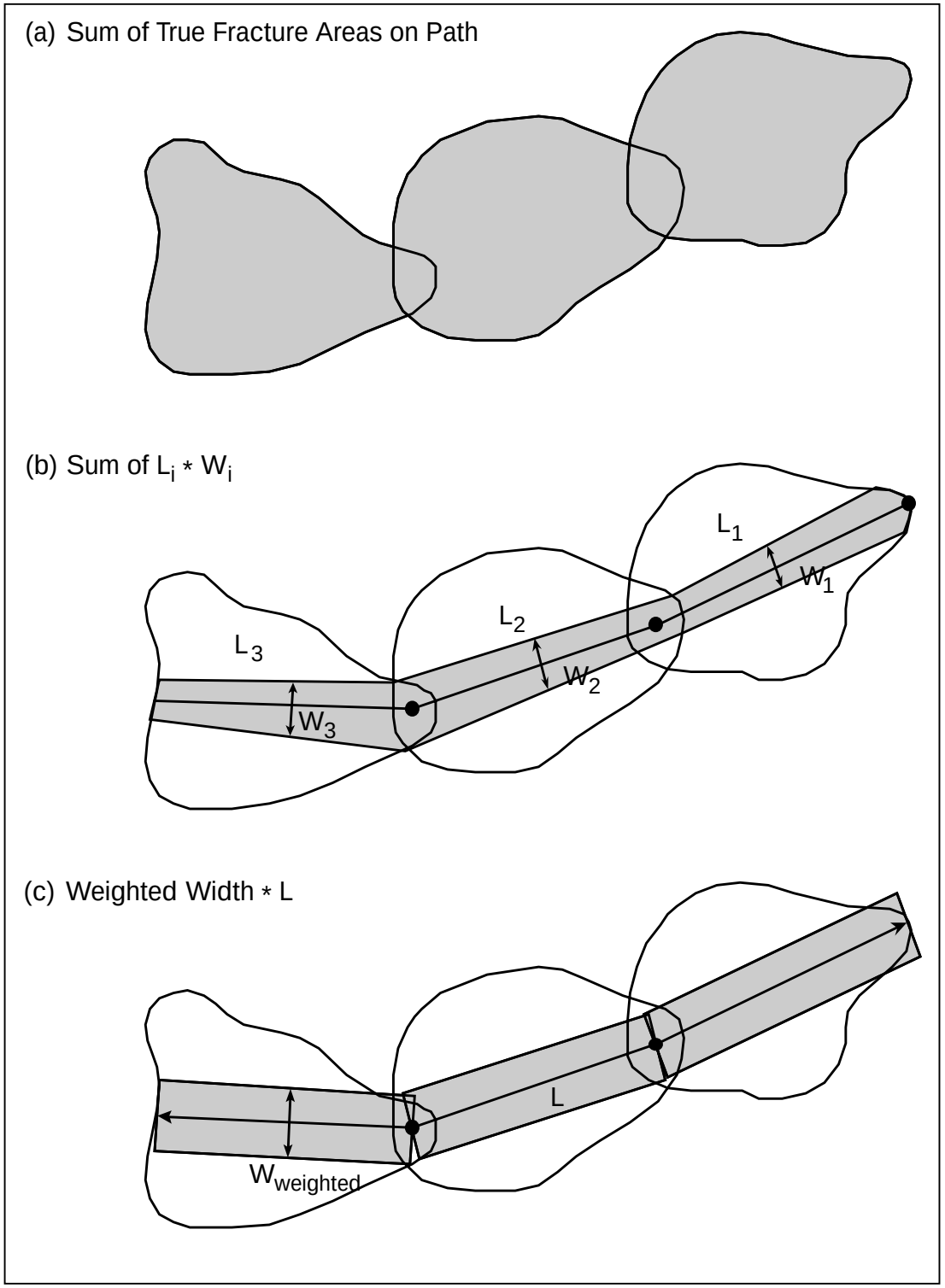

***Figure C-2**. Reactive surface area options.*

Appendix D: Simulation results

This appendix presents for the different cases the tables of results, graphs and figures. The following variables are presented: travel-time, F-factor and Darcy velocity at the canister location. Statistical analysis is carried out on the log10 value of the variables. The following statistical entities are presented: mean, variance, median, standard deviation, range and percentage of canisters that are not connected with a boundary. The 'Mean of realizations in sets' of a variable is the average value of the entities for each realization. The 'pooled data' is the average value of a variable over all realizations.

1 Base case

1.1 Comparison of the ensemble statistics of canister set 1 and canister sets 1, 2, and 3.

Canister Set 1 is chosen arbitrarily among the three-searched canister sets. The comparison of the ensemble statistics and percentiles of canister set 1 and canister sets 1, 2, 3 are presented in Table D1-1 and Table D1-2.

Table D1-1. Comparison of ensemble statistics of canister set 1 and canister sets 1, 2, and 3 (statistics of log10).

Stats	Log10 travel time [yrs]		Log10 F-factor [s/m]		Log10 Darcy's vel. m/s]	
Mean	All sets	Set 1	All sets	Set 1	All sets	Set 1
Mean of realizations in sets	1.51	1.49	12.70	12.67	-10.81	-10.77
Pooled data	1.50	1.49	12.70	12.67	-10.80	-10.77
Variance						
Mean of realizations in sets	0.08	0.08	0.17	0.19	0.72	0.73
Pooled data	0.12	0.12	0.22	0.23	0.76	0.78
Median						
Mean of realizations in sets	1.52	1.50	12.69	12.66	-10.74	-10.72
Pooled data	1.48	1.49	12.68	12.64	-10.73	-10.70
Standard deviation						
Mean of realizations in sets	0.27	0.28	0.40	0.42	0.84	0.85
Pooled data	0.35	0.35	0.47	0.48	0.87	0.88
Range						
Mean of realizations in sets	1.39	1.46	2.33	2.49	4.20	4.04
Pooled data	2.28	2.19	5.61	5.55	6.62	6.53
% non connected canisters						
Pooled data	35.5	37	35.5	37	35.5	37

Table D1-2. Comparison of percentiles of canister set 1 and canister sets 1, 2, and 3 (statistics of log10)**.**

Percentiles	5%	95%	25%	75%
Log10 travel time [yrs]				
All sets	0.99	2.23	1.26	1.70
Set 1	0.97	2.17	1.24	1.70
Log10 F-factor [s/m]				
All sets	12.01	13.44	12.40	12.97
Set 1	11.98	13.40	12.37	12.96
Log10 Darcy flux [m/s]				
All sets	-12.33	-9.49	-11.31	-10.20
Set 1	-12.32	-9.46	-11.31	-10.15

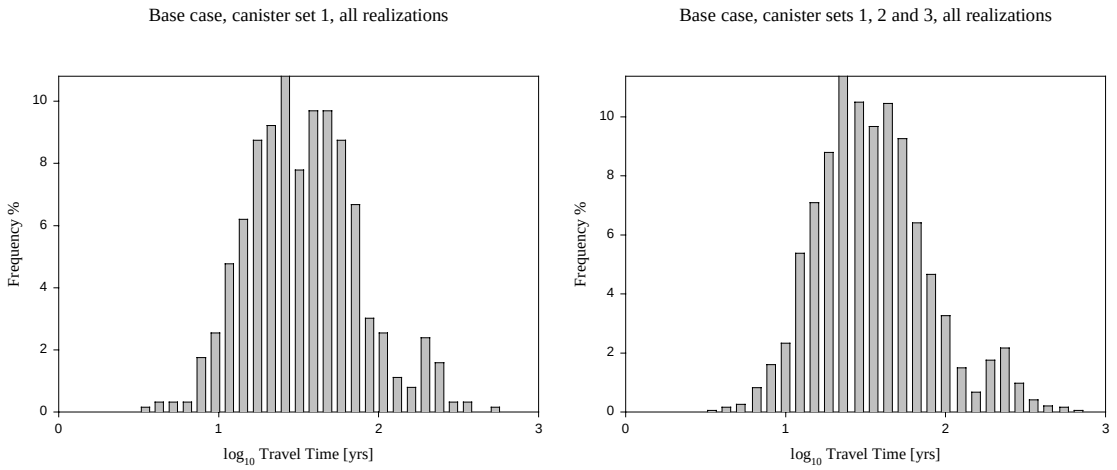

Figure D1-1. *Histograms of travel time, base case, set 1 only and sets 1, 2 and 3.*

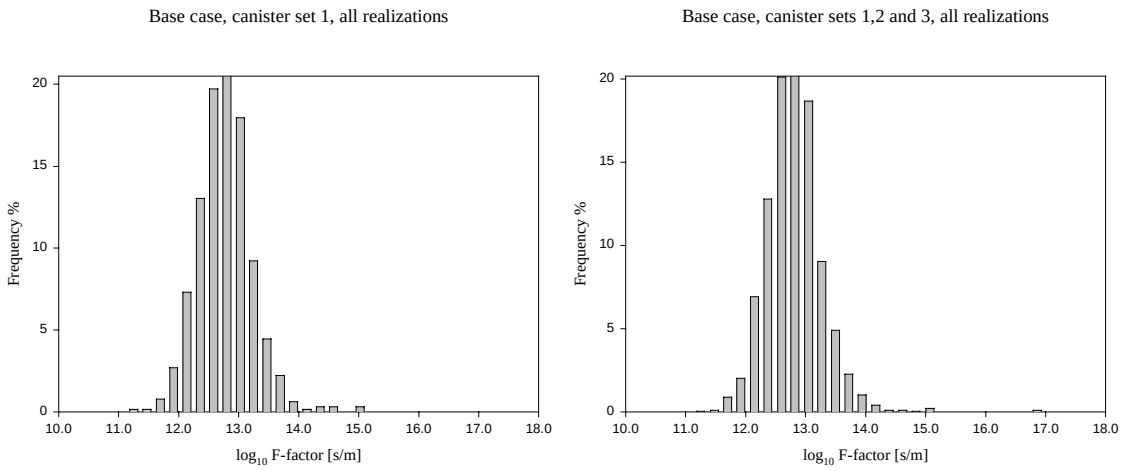

Figure D1-2. *Histograms of F-factor, base case, set 1 only and sets 1, 2 and 3.*

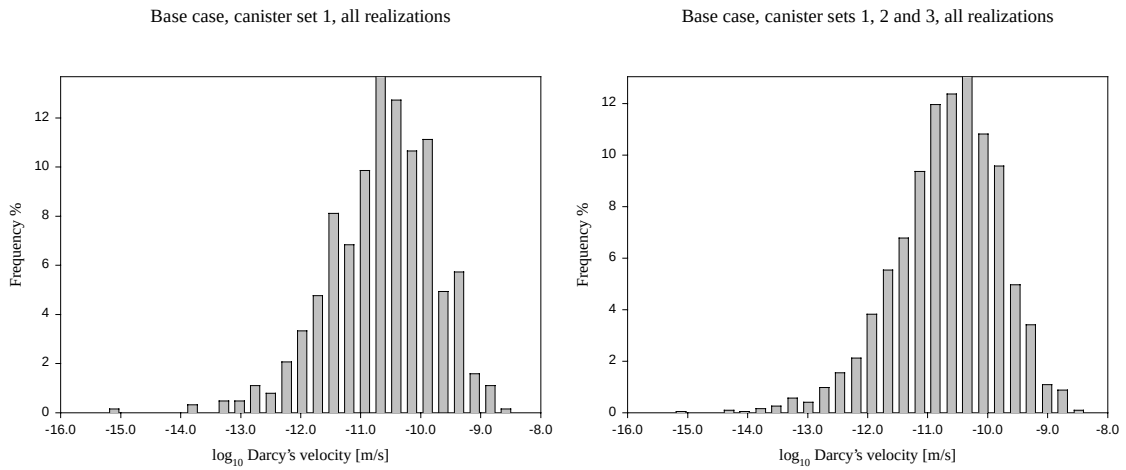

Figure D1-3. *Histograms of Darcy velocity, base case, set 1 only and sets 1, 2 and 3.*

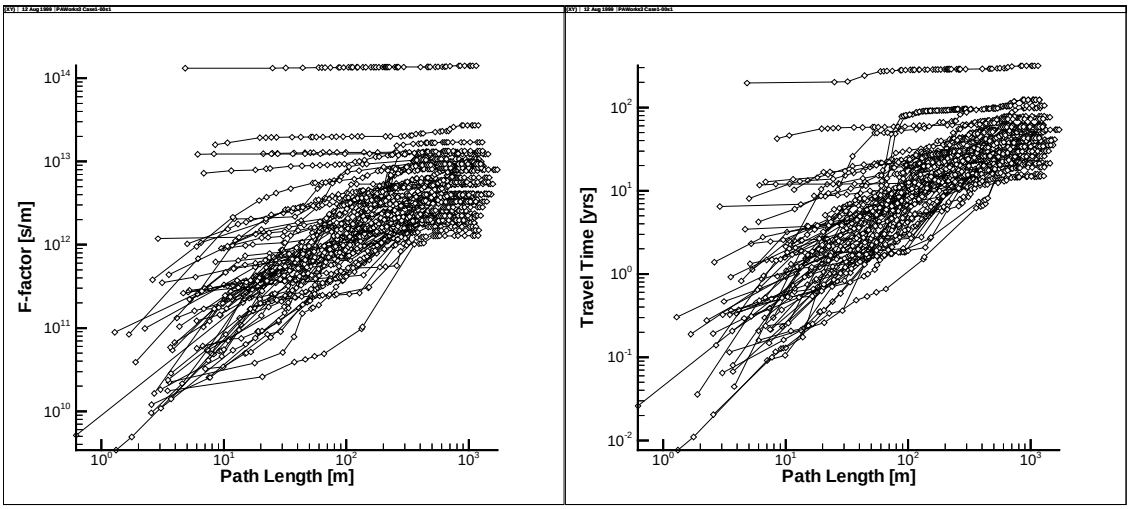

Figure D1-4. *F-factor and travel time, function of the distance from the canister sources. Base case, fracture set 1.*

2 Case 1

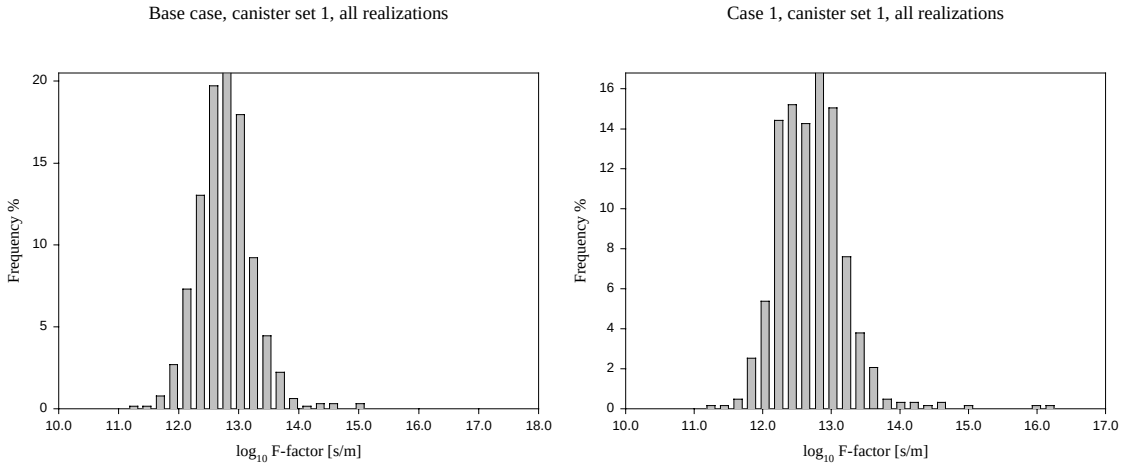

Figure D2-1*. Histograms of F-factor in base case and case 1.*

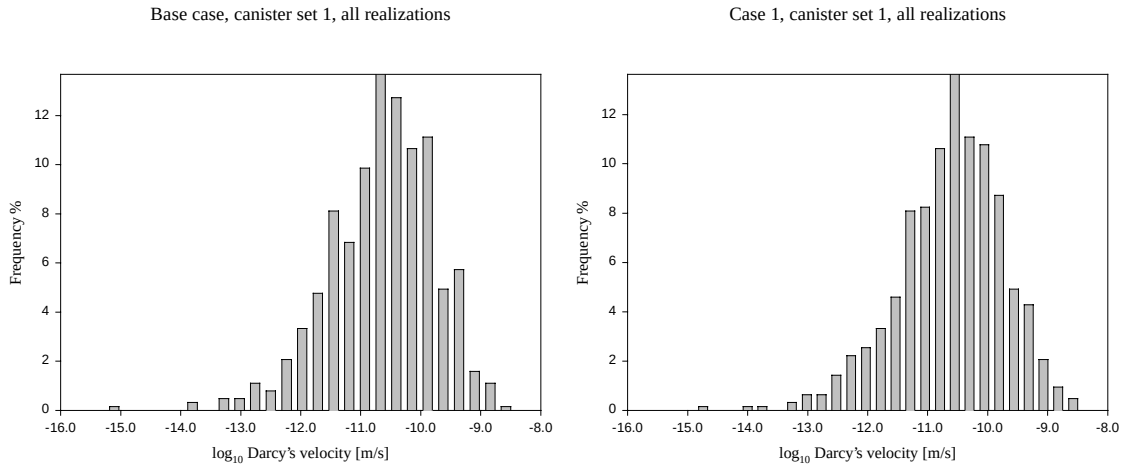

Figure D2-2. *Histograms of Darcy velocity in base case and case 1.*

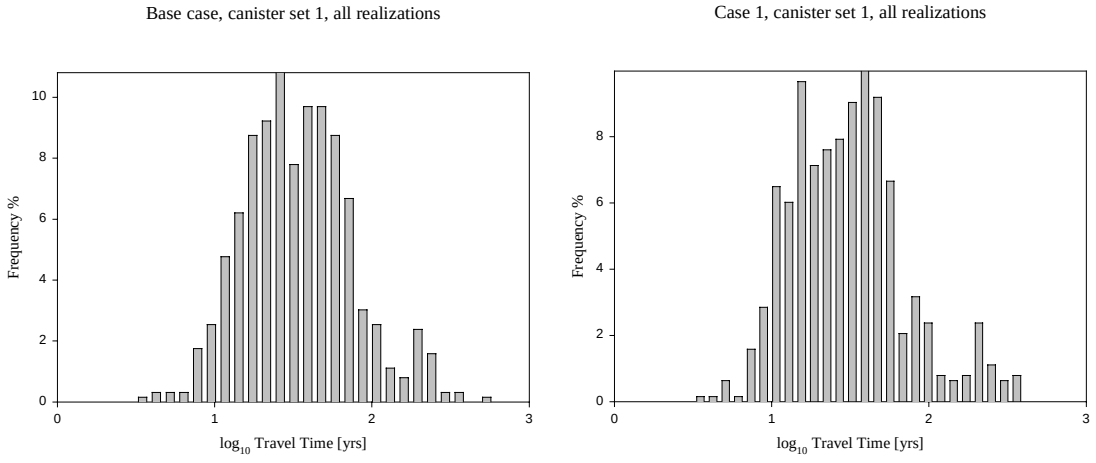

Figure D2-3*.Histograms of travel time in base case and case 1.*

Table D2-1. Statistical analysis of the results of the base case and case 1 (statistics of log10)**.**

Stats	Log10 travel time [yrs]		Log10 F-factor [s/m]		Log10 Darcy´s vel. [m/s]	
Mean	**Base case**	**Case 1**	**Base case**	**Case 1**	**Base case**	**Case 1**
Mean of realizations	1.51	1.44	12.70	12.60	-10.81	-10.73
Pooled data	1.50	1.44	12.70	12.61	-10.80	-10.73
Variance						
Mean of realizations	0.08	0.08	0.17	0.19	0.72	0.75
Pooled data	0.12	0.13	0.22	0.25	0.76	0.78
Median						
Mean of realizations	1.52	1.45	12.69	12.58	-10.74	-10.68
Pooled data	1.48	1.43	12.68	12.58	-10.73	-10.65
Standard deviation						
Mean of realizations	0.27	0.27	0.40	0.42	0.84	0.86
Pooled data	0.35	0.36	0.47	0.50	0.87	0.88
Range						
Mean of realizations	1.39	1.37	2.33	2.47	4.20	4.22
Pooled data	2.28	2.01	5.61	4.94	6.62	6.16
% non connected canisters						
Pooled data	35.6	35.3	35.6	35.3	35.6	35.3

Table D2-2. Percentiles data of the results of the base case and case 1 (statistics of log10)**.**

Percentiles pooled data	5%	95%	25%	75%
Travel time [yrs]				
Base case	0.99	2.23	1.26	1.70
Case 1	0.94	2.23	1.16	1.64
Log10 Cumul. F-factor [s/m]				
Base case	12.01	13.44	12.40	12.97
Case 1	11.91	13.36	12.27	12.88
Log10 Darcy flux [m/s]				
Base case	-12.33	-9.49	-11.31	-10.20
Case 1	-12.37	-9.44	-11.26	-10.10

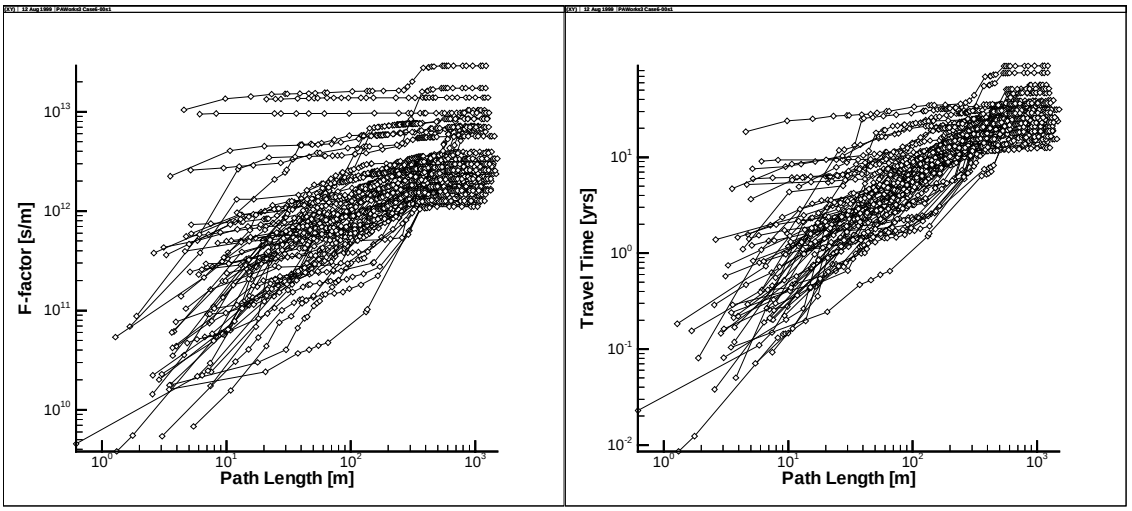

Figure D2-4. *F-factor and travel time, function of the distance from the canister sources. Case 1, fracture set 1.*

3 Case 2

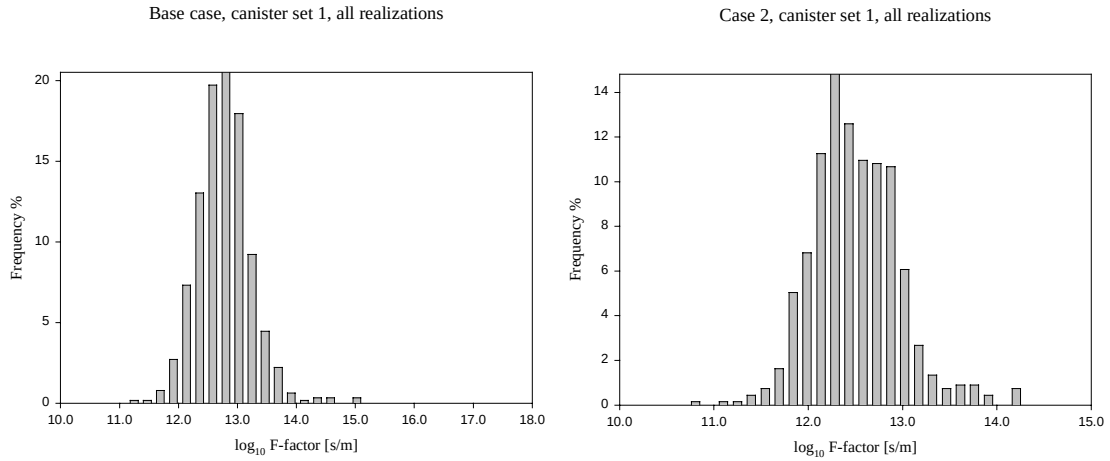

Figure D3-1. *Histograms of F-factor in base case and case 2.*

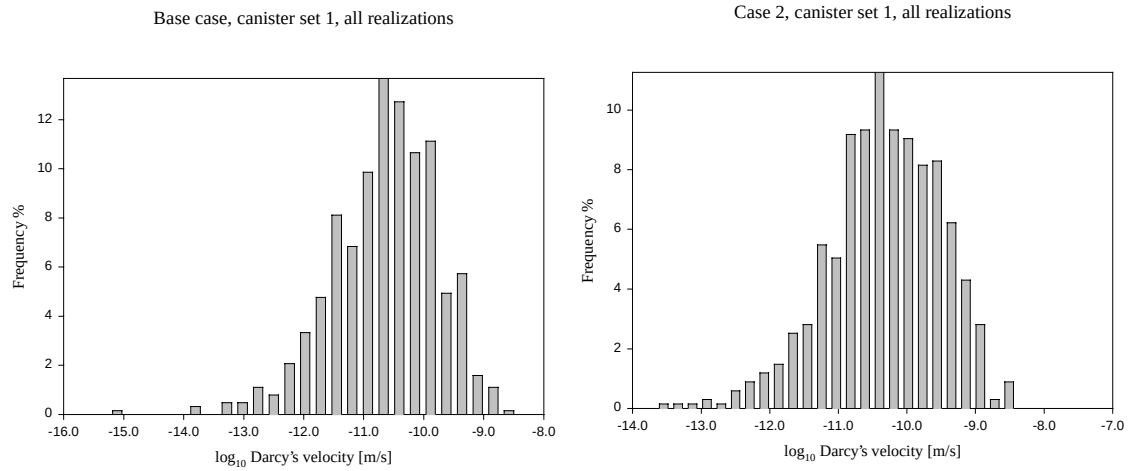

Figure D3-2. *Histograms of Darcy velocity in base case and case 2.*

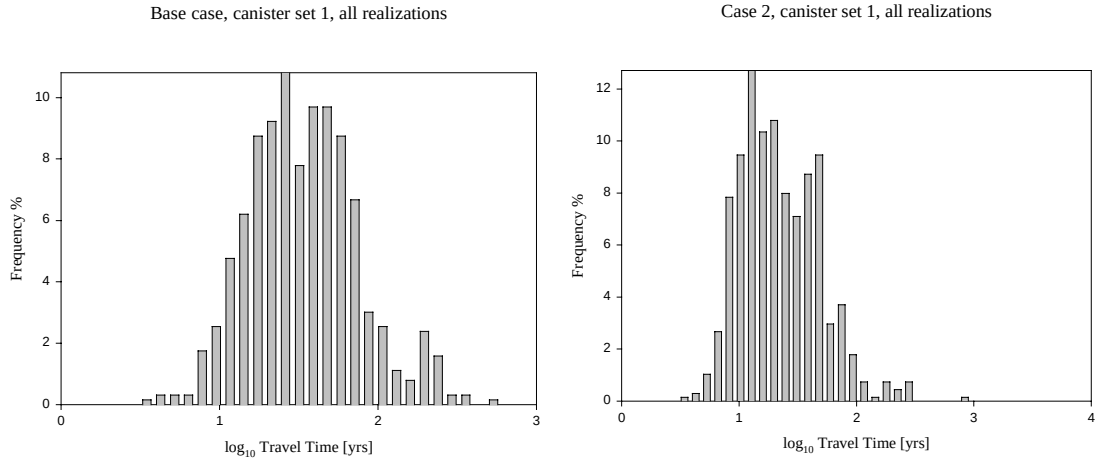

Figure D3-3. *Histograms of travel time in base case and case 2.*

Table D3-1. Statistical analysis of the results of the base case and case 2 (statistics of log10)**.**

Stats	Log10 travel time [yrs]		Log10 F-factor [s/m]		Log10 Darcy´s vel. [m/s]	
Mean	**Base case**	**Case 2**	**Base case**	**Case 2**	**Base case**	**Case 2**
Mean of realizations	1.51	1.30	12.70	12.43	-10.81	-10.43
Pooled data	1.50	1.30	12.70	12.43	-10.80	-10.43
Variance						
Mean of realizations	0.08	0.09	0.17	0.18	0.72	0.66
Pooled data	0.12	0.12	0.22	0.22	0.76	0.68
Median						
Mean of realizations	1.52	1.29	12.69	12.41	-10.74	-10.41
Pooled data	1.48	1.24	12.68	12.40	-10.73	-10.42
Standard deviation						
Mean of realizations	0.27	0.28	0.40	0.41	0.84	0.80
Pooled data	0.35	0.34	0.47	0.47	0.87	0.82
Range						
Mean of realizations	1.39	1.37	2.33	2.31	4.20	3.83
Pooled data	2.28	2.39	5.61	3.70	6.62	5.25
% non connected canisters						
Pooled data	35.6	32.4	35.6	32.4	35.6	32.4

Table D3-2. Percentiles data of the results of the base case and case 2 (statistics of log10)**.**

Percentiles pooled data	5%	95%	25%	75%
Travel time [yrs]				
Base case	0.99	2.23	1.26	1.70
Case 2	0.84	1.87	1.04	1.55
Log10 Cumul. F-factor [s/m]				
Base case	12.01	13.44	12.40	12.97
Case 2	11.75	13.19	12.12	12.72
Log10 Darcy flux [m/s]				
Base case	-12.33	-9.49	-11.31	-10.20
Case 2	-11.86	-9.18	-10.94	-9.81

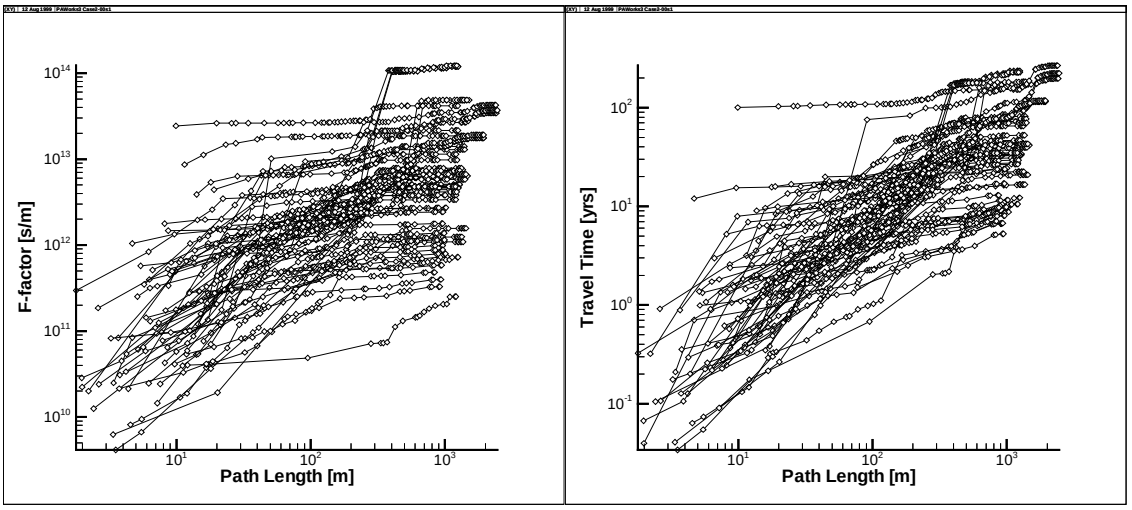

Figure D3-4. *F-factor and travel time, function of the distance from the canister sources. Case 2, fracture set 1.*

4 Case 3

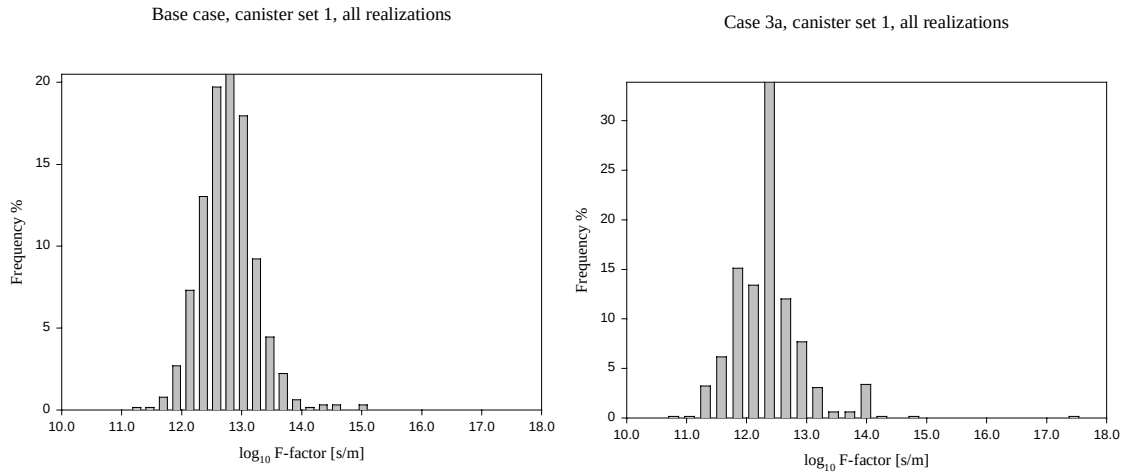

Figure D4-1. *Histograms of F-factor in base case and case 3a.*

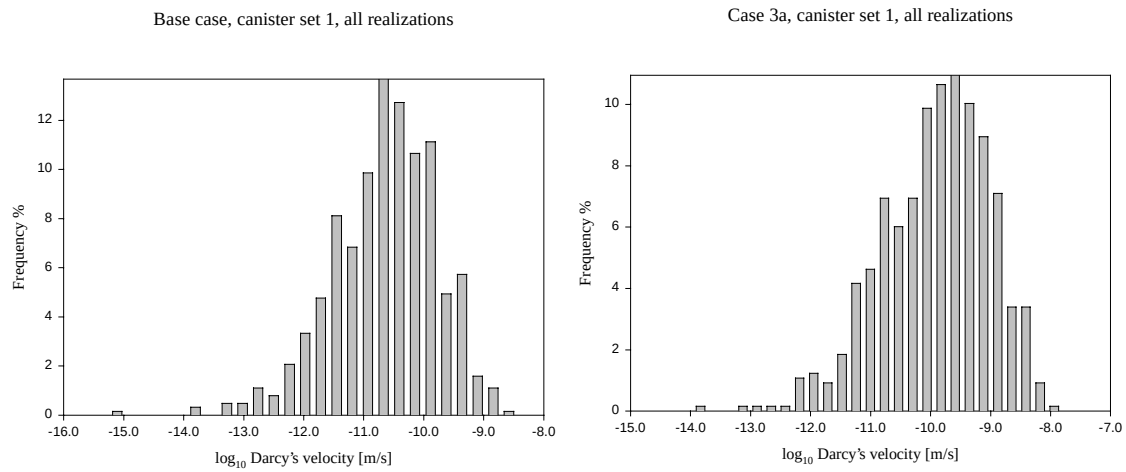

Figure D4-2. *Histograms of Darcy velocity in base case and case 3a.*

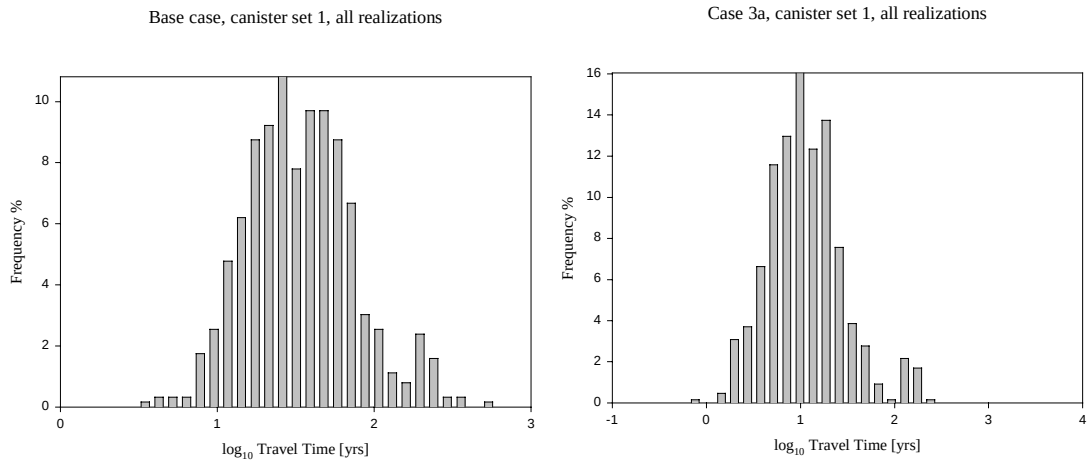

Figure D4-3. *Histograms of travel time in base case and case 3a.*

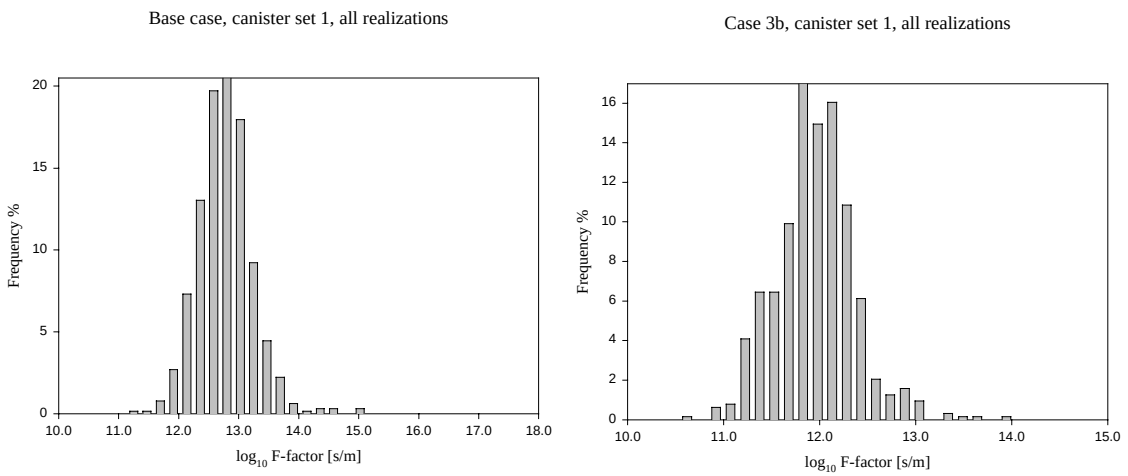

Figure D4-4. *Histograms of F-factor in base case and case 3b.*

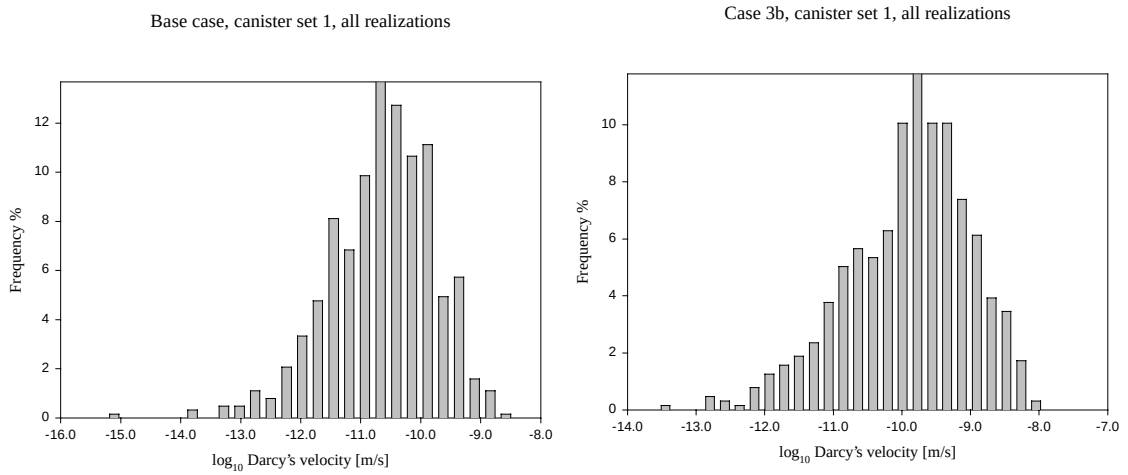

Figure D4-5. *Histograms of Darcy velocity in base case and case 3b.*

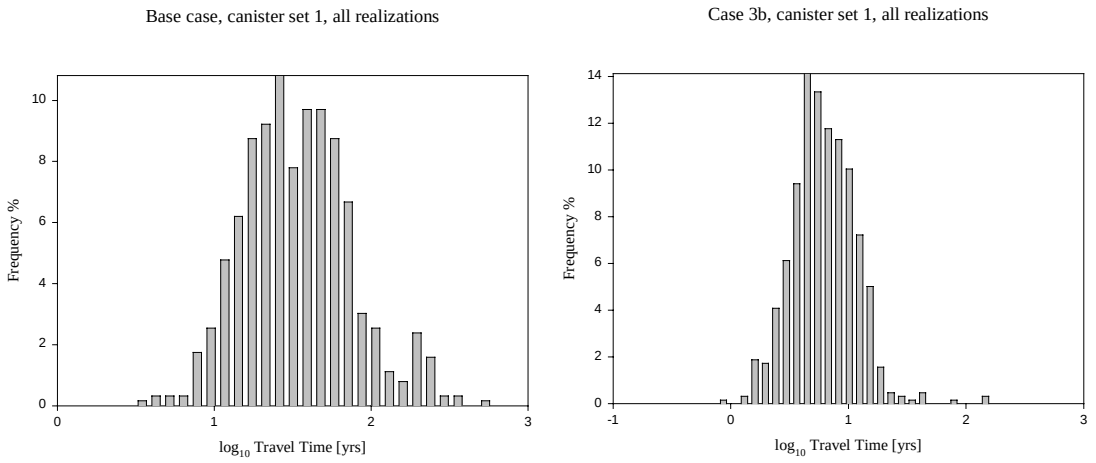

Figure D4-6. *Histograms of travel time in base case and case 3b.*

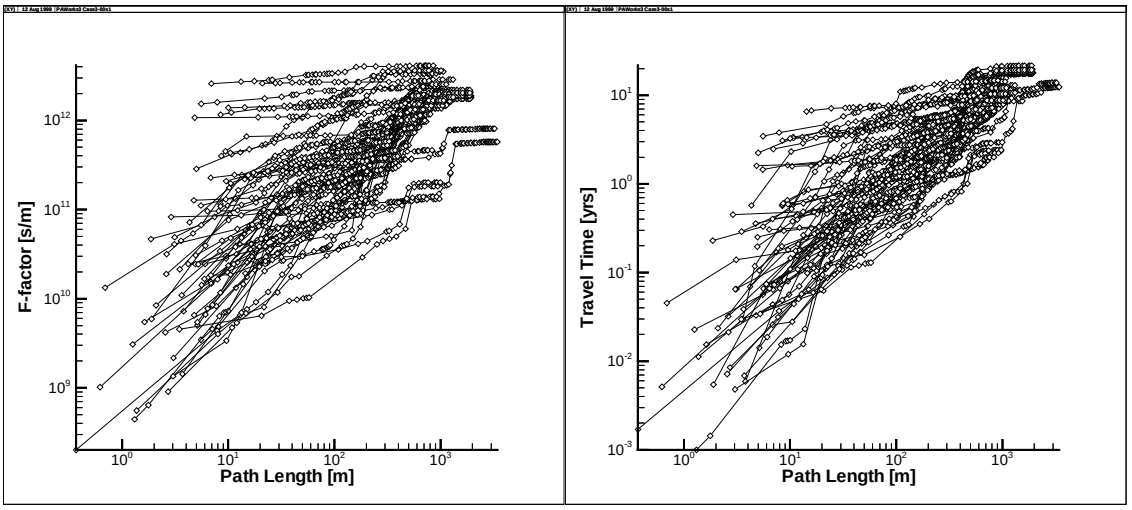

Figure D4-7. *F-factor and travel time, function of the distance from the canister sources. Case 3a, fracture set 1.*

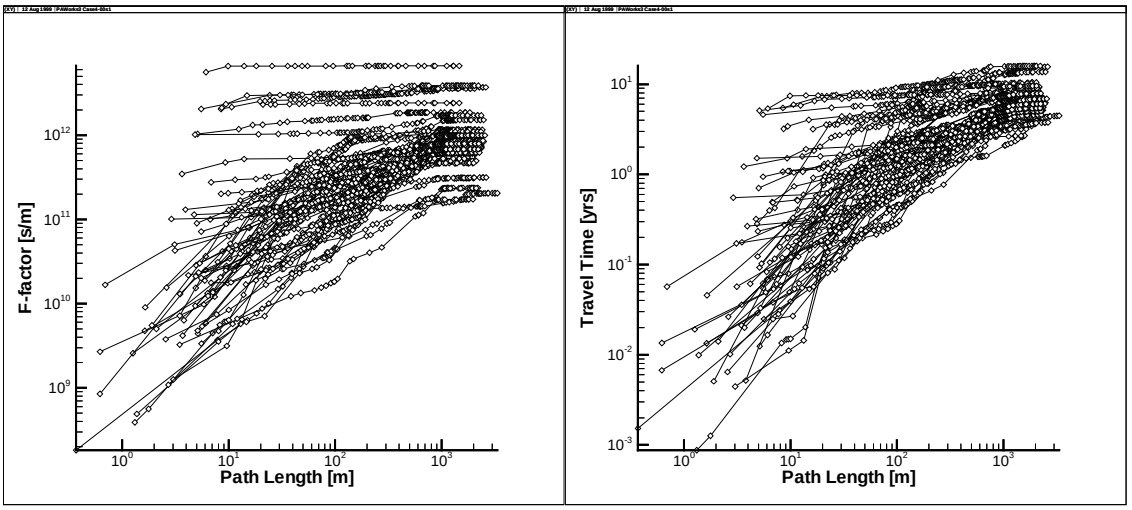

Figure D4-8. *F-factor and travel time, function of the distance from the canister sources. Case 3b, fracture set 1.*

Table D4-1. Statistical analysis of the results of the base case and case 3 (statistics of log10)**.**

Stats	Log10 travel time [yrs]			Log10 F-factor [s/m]			Log10 Darcy´s vel. [m/s]		
Mean	**Base case**	**Case 3a**	**Case 3b**	**Base case**	**Case 3a**	**Case 3b**	**Base case**	**Case 3a**	**Case 3b**
Mean of realizations	1.51	0.97	0.74	12.70	12.21	11.88	-10.81	-10.02	-10.01
Pooled data	1.50	0.99	0.75	12.70	12.23	11.88	-10.80	-10.03	-10.01
Variance									
Mean of realizations	0.08	0.12	0.06	0.17	0.25	0.17	0.72	0.79	0.80
Pooled data	0.12	0.17	0.07	0.22	0.35	0.18	0.76	0.82	0.81
Median									
Mean of realizations	1.52	0.96	0.72	12.69	12.15	11.86	-10.74	-9.92	-9.91
Pooled data	1.48	0.96	0.73	12.68	12.20	11.88	-10.73	-9.94	-9.90
Standard deviation									
Mean of realizations	0.27	0.33	0.24	0.40	0.47	0.41	0.84	0.89	0.89
Pooled data	0.35	0.42	0.27	0.47	0.59	0.43	0.87	0.90	0.90
Range									
Mean of realizations	1.39	1.64	1.32	2.33	2.37	2.22	4.20	4.06	4.14
Pooled data	2.28	3.48	2.23	5.61	6.67	3.78	6.62	5.90	5.40
% non connected canisters									
Pooled data	35.6	35.1	36.3	35.6	35.1	36.3	35.6	35.1	36.3

Table D4-2. Percentiles data of the results of the base case and case 3 (statistics of log10)**.**

Percentiles pooled data	5%	95%	25%	75%
Travel time [yrs]				
Base case	0.99	2.23	1.26	1.70
Case 3a	0.36	1.74	0.71	1.22
Case 3b	0.34	1.16	0.58	0.92
Log10 Cumul. F-factor [s/m]				
Base case	12.01	13.44	12.40	12.97
Case 3a	11.41	13.17	11.86	12.42
Case 3b	11.19	12.55	11.62	12.12
Log10 Darcy flux [m/s]				
Base case	-12.33	-9.49	-11.31	-10.20
Case 3a	-11.57	-8.67	-10.62	-9.37
Case 3b	-11.64	-8.67	-10.58	-9.37

5 Case 4

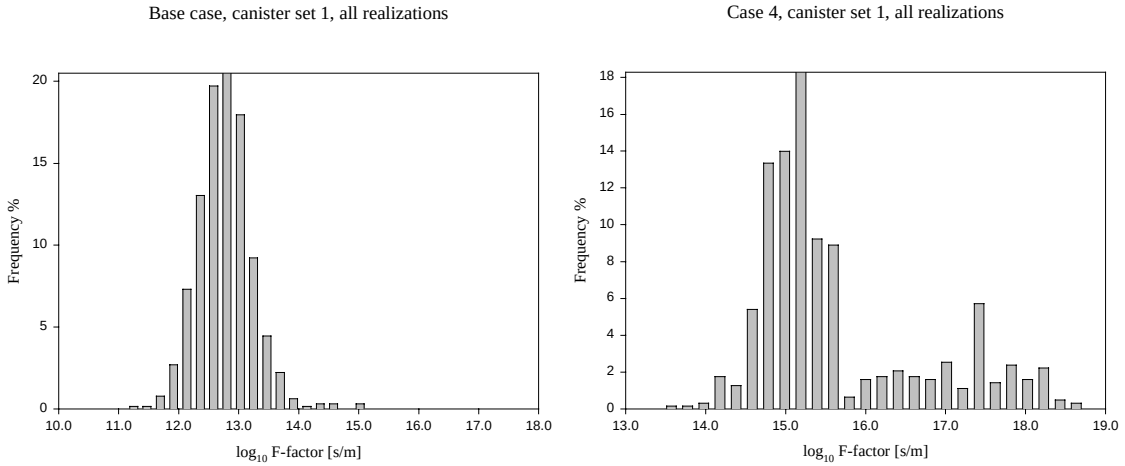

Figure D5-1. *Histograms of F-factor in base case and case 4.*

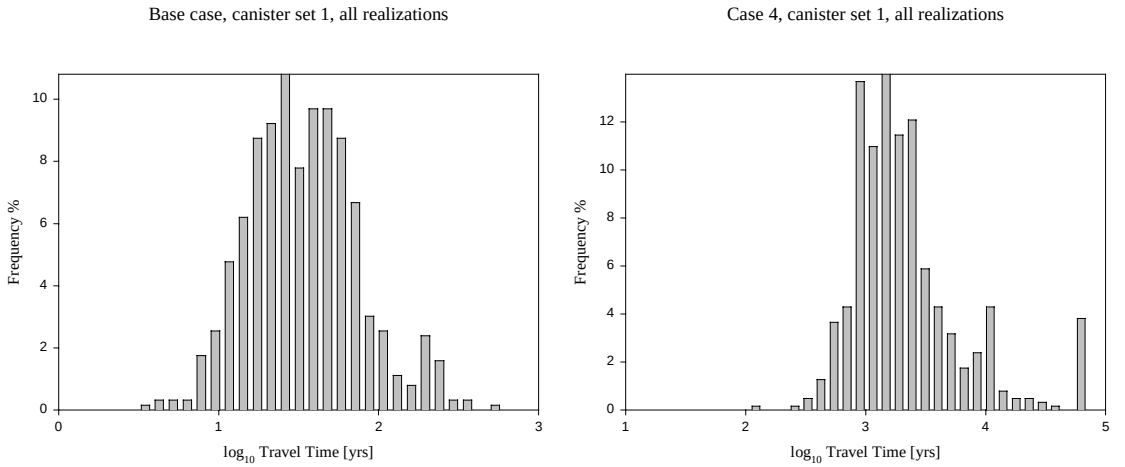

Figure D5-2. *Histograms of travel time, base case and case 4.*

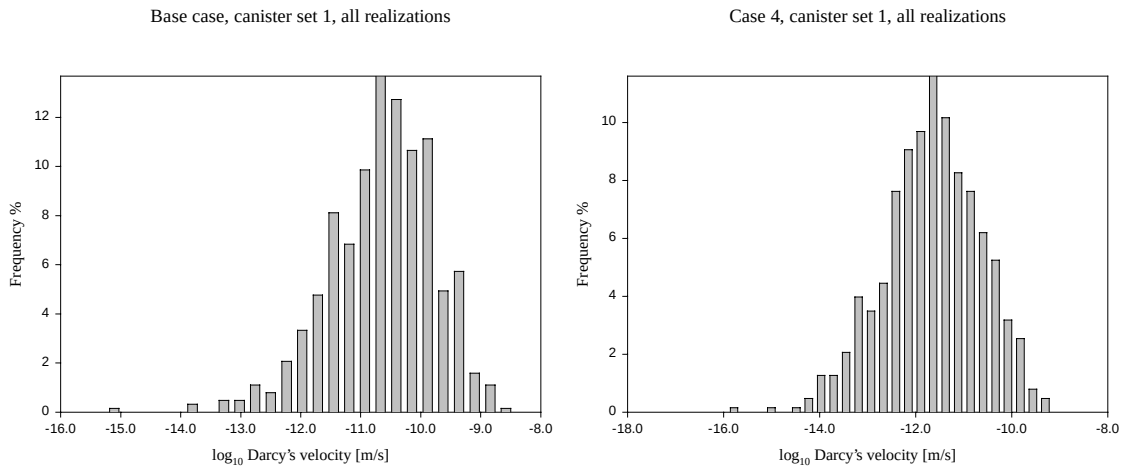

Figure D5-3. *Histograms of Darcy velocity, base case and case 4.*

Table D5-1. Statistical analysis of the results of the base case and case 4 (statistics of log10)**.**

Stats	Log10 Travel time [yrs]		Log10 F-factor [s/m]		Log10 Darcy´s vel. [m/s]	
Mean	**Base case**	**Case 4**	**Base case**	**Case 4**	**Base case**	**Case 4**
Mean of realizations	1.51	3.28	12.70	15.53	-10.81	-11.77
Pooled data	1.50	3.28	12.70	15.54	-10.80	-11.77
Variance						
Mean of realizations	0.08	0.17	0.17	1.08	0.72	0.98
Pooled data	0.12	0.22	0.22	1.14	0.76	1.02
Median						
Mean of realizations	1.52	3.23	12.69	15.15	-10.74	-11.72
Pooled data	1.48	3.19	12.68	15.16	-10.73	-11.74
Standard deviation						
Mean of realizations	0.27	0.37	0.40	1.01	0.84	0.99
Pooled data	0.35	0.47	0.47	1.07	0.87	1.01
Range						
Mean of realizations	1.39	1.51	2.33	3.72	4.20	4.68
Pooled data	2.28	2.71	5.61	5.06	6.62	6.48
% non connected canisters						
Pooled data	35.6	37	35.6	37	35.6	37

Table D5-2. Percentiles data of the results of the base case and case 4 (statistics of log10)**.**

Percentiles pooled data	5%	95%	25%	75%
Log10 travel time [yrs]				
Base case	0.99	2.23	1.26	1.70
Case 4	2.71	4.19	2.96	3.47
Log10 Cumul. F-factor [s/m]				
Base case	12.01	13.44	12.40	12.97
Case 4	14.46	17.80	14.85	16.01
Log10 Darcy flux [m/s]				
Base case	-12.33	-9.49	-11.31	-10.20
Case 4	-13.50	-10.20	-12.41	-11.06

6 Curve fitting of Cumul. F-factor [yrs/m] = function(Travel time [yrs])

Table D6-1. Fitting curve equation parameters for exponential and linear functions.

Case	$Y=aX^b$			$Y=AX$	
	a	b	R^2	A	R^2
Base Case	2597.20	1.18	0.72	3.90×10^5	0.11
Case 1	2932.54	1.14	0.68	4.88×10^4	0.02
Case 2	2177.30	1.23	0.77	1.01×10^4	0.80
Case 3a	2870.58	1.29	0.82	3.56×10^6	0.90
Case 3b	2424.62	1.33	0.72	1.30×10^4	0.20
Case 4	535.30	1.62	0.51	3.79×10^5	0.15

R^2 is the correlation coefficient.